

An observer’s guide to the (Local Group) dwarf galaxies: predictions for their own dwarf satellite populations

Gregory A. Dooley^{1*}, Annika H. G. Peter^{2,3}, Tianyi Yang⁴, Beth Willman⁵,
Brendan F. Griffen¹ and Anna Frebel¹,

¹*Department of Physics and Kavli Institute for Astrophysics and Space Research, Massachusetts Institute of Technology, Cambridge, MA 02139, USA*

²*CCAPP and Department of Physics, The Ohio State University, Columbus, OH 43210, USA*

³*Department of Astronomy, The Ohio State University, Columbus OH 43210, USA*

⁴*Institute of Optics, University of Rochester, Rochester, New York, 14627, USA*

⁵*Steward Observatory and LSST, 933 North Cherry Avenue, Tucson, AZ 85721, USA*

Accepted XXX. Received YYY; in original form ZZZ

ABSTRACT

A recent surge in the discovery of new ultrafaint dwarf satellites of the Milky Way has inspired the idea of searching for faint satellites, $10^3 M_\odot < M_* < 10^6 M_\odot$, around less massive field galaxies in the Local Group. Such satellites would be subject to weaker environmental influences than Milky Way satellites, and could lead to new insights on low mass galaxy formation. In this paper, we predict the number of luminous satellites expected around field dwarf galaxies by applying several abundance matching models and a reionization model to the dark-matter only *Caterpillar* simulation suite. For three of the four abundance matching models used, we find a $> 99\%$ chance that at least one satellite with stellar mass $M_* > 10^5 M_\odot$ exists around the combined five Local Group field dwarf galaxies with the largest stellar mass. When considering satellites with $M_* > 10^4 M_\odot$, we predict a combined 5 – 25 satellites for the five largest field dwarfs, and 10 – 50 for the whole Local Group field dwarf population. Because of the relatively small number of predicted dwarfs, and their extended spatial distribution, a large fraction each Local Group dwarf’s virial volume will need to be surveyed to guarantee discoveries. We compute the predicted number of satellites in a given field of view of specific Local Group galaxies, as a function of minimum satellite luminosity, and explicitly obtain such values for the Solitary Local dwarfs survey. Uncertainties in abundance matching and reionization models are large, implying that comprehensive searches could lead to refinements of both models.

Key words: galaxies: dwarf — galaxies: haloes — methods: numerical

1 INTRODUCTION

Hierarchical structure formation in the Lambda Cold Dark Matter Universe predicts that galaxies like the Milky Way (MW) and M31 are orbited by satellite galaxies (Frenk & White 2012). Observations have long supported this hierarchical accretion model, starting with identifying that the Large Magellanic Cloud (LMC) and Small Magellanic Cloud (SMC) are within close proximity of the Milky Way (Shapley 1922, 1924). An additional nine MW satellites with luminosity $L_* > 10^5 L_\odot$, the classical dwarfs, were discovered next, followed by a class of satellite galaxies with luminosity

$10^3 < L < 10^5 L_\odot$, the ultrafaint dwarfs (UFDs), initially discovered in the Sloan Digital Sky Survey (Willman et al. 2005b; Zucker et al. 2006a; Belokurov et al. 2006, 2007, 2008, 2010; Irwin et al. 2007; Walsh et al. 2007). Even smaller “hyperfaint” galaxies ($L_* < 10^3 L_\odot$) have also been discovered, galaxies so tiny they can only be found very near the Sun (Willman et al. 2005a; Zucker et al. 2006b; Belokurov et al. 2009). The window into UFD and hyperfaint satellites of the MW is opening up dramatically, as the Dark Energy Survey, PanSTARRS, ATLAS, and MagLiteS surveys have found ~ 20 new UFD satellite candidates in the past two

* e-mail: gdooley@mit.edu

years (Bechtol et al. 2015; Drlica-Wagner et al. 2015; Kim et al. 2015; Kim & Jerjen 2015; Koposov et al. 2015; Laevens et al. 2015; Martin et al. 2015; Luque et al. 2016; Torrealba et al. 2016; Drlica-Wagner et al. 2016), and will likely continue to find more.

These recent discoveries, along with follow up observations, have opened the door to better understand low mass galaxy formation. Whereas classical dwarfs have recent star formation, many UFDs have been confirmed to be “fossil” galaxies, meaning that $> 70\%$ of their stars formed before reionization (Brown et al. 2012, 2014a,b). Consequently, they contain very old stellar populations (Kirby et al. 2008; Norris et al. 2010; Frebel & Bromm 2012) and are ideal targets to learn about early universe galaxy formation. Both classical dwarfs and UFDs serve as probes on the interplay of ionizing radiation, supernova feedback, star formation, and halo size. Low-mass galaxies are susceptible to losing gas from reionization and supernovae, which can turn them into fossil galaxies or even leave them entirely dark. However, due to strong environmental effects on dwarf galaxy evolution, and halo-to-halo variation, a large sample size of dwarf galaxies in different environments is necessary to probe the halo size scale where these effects begin.

To constrain star formation models in dwarf galaxies, there is significant value in even just the number counts of UFDs and classical dwarfs. Completeness in discovery around the MW will further refine the so-called “missing satellite problem” (Moore et al. 1999; Klypin et al. 1999) and its many proposed solutions, which come in both baryonic and dark-matter flavors. Baryonic solutions include the effects described above, to suppress the formation of stars in small dark-matter halos. With a large sample of UFDs, we can test abundance-matching-derived $M_* - M_{\text{halo}}$ relationships to much smaller mass scales than those for which the relations were observationally inferred. A change in the slope or scatter of abundance-matching relations would have significant implications for the drivers of star-formation efficiency in small galaxies.

Discovering a large sample of UFDs is also critical in revealing a diversity of chemical enrichment pathways, such as r-process enhancement or lack thereof (Ji et al. 2016). By finding more UFDs in particular, we should discover older and more metal poor stellar populations. We also create more opportunities to measure internal halo structure, which has important implications on the cusp/core debate (de Blok 2010) and the nature of dark matter (Elbert et al. 2015; Dooley et al. 2016).

Given the importance of finding more low-mass galaxies, it is natural to consider searching for them beyond the MW. Already, many satellites have been discovered around Andromeda (Zucker et al. 2004, 2007; McConnachie et al. 2008, 2009; Majewski et al. 2007; Irwin et al. 2008; Martin et al. 2009; Bell et al. 2011; Slater et al. 2011; Richardson et al. 2011), and around a handful of nearby galaxies and clusters (Jang & Lee 2014; Sand et al. 2014; Crnojević et al. 2016). Several of these recent discoveries have been of dwarf galaxy satellites of dwarf galaxies themselves (Sand et al. 2015; Carlin et al. 2016, e.g.). This opens the question if there could exist satellites around isolated dwarf galaxies within the Local Group itself. Due to a lower mass host, they would experience weaker environmental influences than those in the MW or M31. Tidal and ram pressure stripping

are reduced, so satellites would retain more of their original stars, gas, and dark matter. Reionization would also proceed differently, as the nature of the closest source of ionizing photons would change. These differences would provide an opportunity to better isolate the internal drivers of low mass galaxy formation. While isolated galaxies would have even weaker environmental effects, hierarchical galaxy formation dictates that the density of low-mass galaxies is greater around a larger galaxy than in areas of complete isolation.

We therefore set out to characterize the abundance of satellites around Local Group field dwarfs, or “dwarf-of-dwarf”, systems as a guide to current and future surveys. We predict the number of satellites of dwarf galaxies given simple, physically motivated prescriptions for how dwarfs populate dark-matter halos in the canonical cold-dark-matter model. We outline observational strategies for finding dwarf-of-dwarf satellites and discuss how to interpret observations in light of models for star formation in small halos. We focus specifically on the satellite systems of Local Group field dwarf galaxies, because the proximity of these galaxies enables the discovery of very low luminosity satellites as overdensities of resolved stars. We include specific predictions for the fields of view of the Solitary Local dwarfs survey (Solo), a recent survey of all isolated dwarfs within 3 Mpc of the Milky Way (Higgs et al. 2016). Though the main goals of the Solo survey do not include finding satellites, it likely already has at least one lurking in its data. Furthermore, our results can be used to estimate the number of dwarf-of-dwarf satellites which Sagittarius, Fornax, and the SMC brought into the Milky Way at infall. Values for the LMC, which is larger than the mass range of hosts we consider in this paper, will be presented in future work.

Sales et al. (2013) and Wheeler et al. (2015) have made similar calculations to ours, predicting the probability of an UFD satellite around a dwarf galaxy within a $10^{10} M_{\odot}$ dark matter halo, as 40–50% and 35%, respectively. We perform a more in-depth study over a larger parameter space, finding the likelihood of satellites existing around dwarf galaxy hosts of a range of host masses, the mean number of satellites around hosts as a function of satellite stellar mass, and the full probability distribution of the number of satellites around known field dwarfs. Due to uncertainty in the $M_* - M_{\text{halo}}$ relationship for low luminosity systems, we use a variety of abundance matching models rather than just one model for star formation. We additionally determine the sensitivity of predictions on input parameters, including reionization, a study not previously conducted.

Our paper is organized as follows: In Section 2, we outline our methods for modeling satellite populations in isolated dwarf galaxies. In Section 3, we validate our methods with predictions for the Milky Way, predict how many luminous satellites should exist around dwarf galaxies, and compute the probability of finding one or more satellites per host. In Section 4, we provide a model for the number of satellites within a line of sight as a function of field of view, and comment on observational strategies. In Section 5, we show how sensitive our predictions are to uncertainties. Finally, we summarize our key findings and present a plan for future directions in Section 6.

2 METHODS

To predict the number of luminous satellites of Local Group dwarf galaxies, we apply a suite of abundance matching models and a parameterized reionization recipe to dark-matter-only simulations of Milky Way-like halos (and their surrounding environments). This simple scheme is fast to implement, unlike fully hydrodynamic simulations, and allows us to quickly explore different models for how dwarf galaxies populate halos. With this scheme, we can generate many realizations of dwarf satellite systems, so we can define a probability distribution for the satellite populations for each model.

We use dark-matter only simulations to predict the subhalo mass functions (SHMFs) of satellites around isolated field dwarfs in the vicinity of a Milky Way-mass galaxy, and use these SHMFs to generate Poisson samples of subhalos around each dwarf galaxy host. Next, we model the effects of reionization by assigning each subhalo a probability that it hosts stars or remains dark. We then apply abundance matching prescriptions from the literature to assign stellar mass to the luminous subhalos.

In the following subsections we elaborate on the simulations, abundance matching models, reionization methodology, and mass functions used.

2.1 Caterpillar Simulation Suite

We use a sample of 33 high particle resolution ($m_p = 3 \times 10^4 M_\odot$) and high temporal resolution (320 snapshots) zoom-in simulations of Milky Way-sized galaxies from the *Caterpillar* simulation suite (Griffen et al. 2016b). The simulations are used to determine the typical SHMF, radial dependence of the SHMF, subhalo infall distribution times, and dark fraction of halos due to reionization. We perform these calculations on both the Milky Way sized host halo and smaller nearby field halos. We consider field galaxies as halos with virial mass between 10^{10} and $10^{11.5} M_\odot$ at $z = 0$ that are outside of the virial radius of the MW sized host, and within the uncontaminated volume of each simulation. We choose the mass range to reflect that of real Local Group field galaxies. In total there are 148 field halos across the 33 simulations.

All self-bound haloes are found using a modified version of the ROCKSTAR HALO FINDER (Behroozi et al. 2013b) which includes full iterative unbinding to improve halo finding accuracy, as described in Griffen et al. (2016b). Merger trees were produced by ROCKSTAR CONSISTENT TREES (Behroozi et al. 2013a). Any mention of *virial* refers to the Bryan & Norman (1998) definition of the virial radius, R_{vir} , which at $z = 0$ for our cosmological parameters is the radius such that the mean enclosed halo density is 104 times the critical density of the universe, $\rho_c = 3H_0^2/8\pi G$. M_{vir} refers to the gravitationally bound mass within R_{vir} , and any mention of R_Δ or M_Δ refers to the radius and mass of a halo where the mean enclosed density is Δ times the critical density.

2.2 Abundance Matching Models

Abundance matching (AM) is a technique employed to determine an approximate stellar mass to halo mass ($M_* - M_{\text{halo}}$) relationship for galaxies. Given a set of observed

galaxies within a volume down to some luminosity completeness limit, galaxies are matched in a one-to-one fashion with dark matter halos from a simulation of the same volume. They traditionally assume a monotonic relationship of stellar mass and dark matter halo mass to create a function $M_*(M_{\text{halo}})$ that satisfies the condition

$$\int_{M_*(m_1)}^{M_*(m_2)} \frac{dN_*}{dM} (M_*) dM_* = \int_{m_1}^{m_2} \frac{dN}{dM} (M_{\text{halo}}) dM_{\text{halo}} \quad (1)$$

where $\frac{dN_*}{dM} (M_*)$ is the differential stellar mass function, and $\frac{dN}{dM}$ is the differential halo mass function (Yang et al. 2003; Vale & Ostriker 2004; Kravtsov et al. 2004; Tasit-siomi et al. 2004; Vale & Ostriker 2006; Guo et al. 2010; Moster et al. 2010; Kravtsov 2010; Wang & Jing 2010; Yang et al. 2012; Moster et al. 2013; Behroozi et al. 2013b; Brook et al. 2014; Garrison-Kimmel et al. 2014). For galaxies with $M_* > 10^8 M_\odot$, abundance matching relationships produce relatively consistent results with each other. However, at smaller masses, incomplete surveys of low luminosity galaxies and a more stochastic process of star formation in halos leads to larger uncertainty in the $M_* - M_{\text{halo}}$ relationship. We highlight this in Fig. 2, showing the relationship for several recently proposed models. Different extrapolations of the function down to low masses, how stochastic star formation is, and what simulations and observations were compared lead to very different predictions. We briefly describe each of the models and details on their implementation in the following paragraphs. The names in bold indicate how we refer to the models in the rest of the paper.

Moster: Moster et al. (2013) match observed stellar mass functions at different redshifts from Sloan Digital Sky Survey (SDSS), Spitzer Space Telescope, Hubble Space Telescope and Very Large Telescope to dark matter halos in the Millennium (Springel et al. 2005) and Millennium-II (Boylan-Kolchin et al. 2009) simulations to produce a redshift dependent AM model. For subhalos, they define M_{halo} as M_{200}^{infall} , the mass of a halo at first infall enclosed by a volume that is $200 \times \rho_c$. To account for the redshift dependence in their model, we find the infall time distribution of all $z = 0$ satellites in *Caterpillar* and use it to assign random infall times to our subhalos in subsequent analysis. We investigate whether the infall time distribution changes when considering different ranges of subhalo masses, but find at most a weak dependence on subhalo mass that results in a $< 1\%$ influence on our final estimates of luminous satellites. We therefore use an infall time distribution independent of subhalo mass. We find the distributions for satellites in MW-sized halos and field halos are consistent with each other, as seen in Fig. 1, and match well in form to fig. 3 of Barber et al. (2014). Barber et al. (2014) finds that when selecting only subhalos which form stars as opposed to all subhalos, the mean infall time is shifted ~ 1 Gyr earlier. This adjustment makes little difference to the predictions made by the Moster model, as discussed in Section 5, so we use the distribution for all subhalos.

Behroozi: Behroozi et al. (2013b) deduce stellar mass functions from $z = 0$ to $z = 8$ with results from SDSS, GALEX, and PRIMUS surveys. They match these to halo mass functions from the *Bolshoi* (Klypin et al. 2011), *MultiDark* (Riebe et al. 2011), and *Consuelo* simulations to produce a redshift dependent $M_* - M_{\text{halo}}$ model which defines M_{halo} as $M_{\text{vir}}^{\text{peak}}$, the maximal virial mass achieved by the

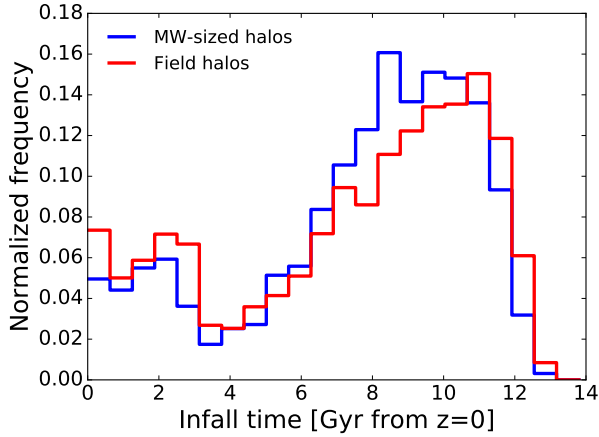


Figure 1. Infall time distribution for all $z = 0$ subhalos averaged over all MW-sized hosts in 33 *Caterpillar* simulations, and over all field halos. Time is given by the duration between infall and $z = 0$. The distribution does not vary significantly with host halo mass, nor range of subhalo mass.

subhalo over its history. We show the function in Fig. 2, but do not include the model in our results since it overpredicts the abundance of low-mass galaxies and is otherwise incorporated in the next two models.

GK14: Garrison-Kimmel et al. (2014) match galaxies from the SDSS to dark matter halos in their ELVIS suite to create an AM model of the same functional form as that in Behroozi et al. (2013b), but with a steeper logarithmic slope on the low mass end. They identify that Behroozi et al. (2013b) overestimates the number of galaxies with $M_* < 10^{8.5} M_\odot$ at $z = 0$ due to using a now outdated stellar mass function, and correct for it. Below the completeness limit of $M_* = 10^8 M_\odot$, GK14 extrapolates their relationship with a constant slope. Like Behroozi, they define M_{halo} as $M_{\text{vir}}^{\text{peak}}$. For their cosmology, R_{vir} encloses a volume that has density $97 \times R_{\text{vir}}$, making it marginally larger than $R_{\text{vir}} = R_{104}$ in our cosmology. We find the discrepancy small enough to not take into account in detail.

GK16: Many hydrodynamic simulations have demonstrated that there can be significant scatter about a mean $M_* - M_{\text{halo}}$ relationship (Munshi et al. 2013; Sawala et al. 2015; Wheeler et al. 2015; O’Shea et al. 2015). The scatter increases towards lower masses, making the default abundance matching assumption of a monotonic relationship problematic particularly for dwarfs (Power et al. 2014; Ural et al. 2015). Garrison-Kimmel et al. (2016) explicitly model the scatter, proposing a range of stochastic abundance matching relationships. They build off the GK14 model, changing the slope of the best fit relationship as a function of the 1-sigma level of lognormal scatter, σ_{scat} . With higher levels of scatter, more galaxies are upscattered above the observed completeness luminosity than are scattered below it due to the increasing abundance of DM subhalos at lower masses. Consequently, their mean $M_* - M_{\text{halo}}$ relationship must be steeper and thereby lower for low mass halos. They match galaxies in the Local Group to the ELVIS suite down

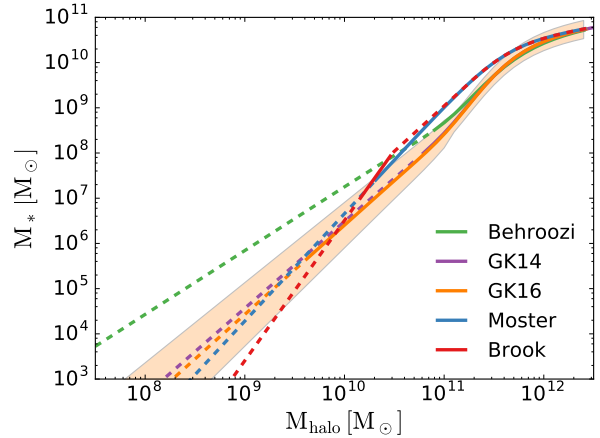


Figure 2. Abundance matching derived stellar mass-halo mass relationships for several recent models. Solid lines indicate ranges of each model where they were matched to observations, dashed lines indicate ranges of extrapolation. The large variation in predictions, particularly for halos with $M_{\text{halo}} < 10^{10} M_\odot$, results in very different predictions for the number of low mass satellite galaxies that could be discovered in the Local Group. While similar, the definition of M_{halo} is different for each of the models, making purely visual comparisons between functions not entirely accurate. The mass definitions are listed in Table 1. The shaded area around GK16 indicates the $\pm 1\sigma$ lognormal scatter we implement.

to a completeness limit of $M_* > 4.5 \times 10^5 M_\odot$, and define M_{halo} as $M_{\text{vir}}^{\text{peak}}$ as in GK14.

Our default implementation of this model is to use the “growing scatter” model, in which σ_{scat} grows for decreasing halo masses. We make this choice because simulations such as those of O’Shea et al. (2015) and Sawala et al. (2015) support a growing scatter more than a constant scatter. The level of growth is dictated by a parameter, γ , as in Eq. (3) of Garrison-Kimmel et al. (2016). We choose a default value of $\gamma = -0.2$. In Section 5, we discuss how results change when varying γ . We implement the scatter by sampling a lognormal offset from the mean $M_* - M_{\text{halo}}$ relationship randomly from a Gaussian of width $\sigma_{\text{scat}}(M_{\text{halo}})$ for each subhalo considered.

Brook14: Brook et al. (2014) proposes an even steeper slope than Garrison-Kimmel et al. (2014), which, when extrapolated to $M_* < 10^7 M_\odot$, estimates lower stellar masses for a fixed DM mass. They match observed galaxies in the Local Group to the CLUES simulation suite (Gottloeber et al. 2010). Instead of $M_{\text{vir}}^{\text{peak}}$, they define M_{halo} as M_{350}^{peak} , the peak mass achieved by a subhalo measured within a volume that has density $350 \times \rho_c$. We implement their model which has an $M_* - M_{\text{halo}}$ log-log slope of 3.1, and normalization factor $M_0 = 79.6$. For stellar masses $M_* > 10^8 M_\odot$, the Brook model is unspecified, so we linearly interpolate values in log-log space between $M_* = 10^8 M_\odot$ in the Brook model and $M_* = 3 \times 10^9 M_\odot$ in the Moster model, then switch to values from Moster. No satellites considered in this paper have $M_* > 10^8 M_\odot$, but a few host galaxies do, and a function to estimate their dark matter halo mass from stellar mass is needed.

2.3 Reionization

UV photons emitted by the first stars during reionization are able to ionize hydrogen atoms and prevent sufficient cooling and gas accretion needed for star formation (Efstathiou 1992; Thoul & Weinberg 1996; Gnedin 2000; Wiersma et al. 2009; Pawlik & Schaye 2009). In low mass halos, they can also heat gas enough to gravitationally escape, sometimes before any star formation begins (Barkana & Loeb 1999; Shapiro et al. 2004; Okamoto et al. 2008). The combination of effects renders many halos entirely dark, an effect recently simulated and emphasized in Sawala et al. (2013, 2015, 2016). Simply assuming that all dark matter subhalos host luminous galaxies would therefore wildly overestimate the number of visible satellites (Bullock et al. 2000; Somerville 2002; Benson et al. 2002).

We model the effects of reionization by randomly assigning halos to host stars or remain dark with probabilities that depend on the halo’s mass. Using data obtained from Barber et al. (2014), we produce a smoothed curve indicating the fraction of halos that are luminous at $z = 0$ as a function of M_{200}^{infall} , as plotted in Fig. 3. The function follows from a semi-analytic model applied to the level-2 halos of the Aquarius simulation suite (Springel et al. 2008). The model has reionization proceeding from $z = 15$ to $z = 11.5$. Below a redshift dependent filtering mass, it models photoevaporation by removing baryons from halos. Full details of the semi-analytic model are given in Starkenburg et al. (2013).

Since the abundance matching models use different definitions for M_{halo} , we produce a different luminous fraction function for each definition. We do this by randomly assigning halos to be dark or luminous in our simulation according to their M_{200}^{infall} , then collecting the values of $M_{\text{vir}}^{\text{peak}}$ and M_{350}^{peak} for those same halos in the merger tree. Repeating the random assignments for many instances generates a list of dark and luminous halos paired with each mass definition, which is then turned into the desired function. In all cases, reionization suppresses the number of satellites with $M_* < 10^5 M_\odot$, but has little effect suppressing larger systems.

Many details of reionization, including the redshift of occurrence, environmental effects, H_2 shielding, and the efficiency of photoevaporation, remain uncertain (Oñorbe et al. 2016), which adds variability to the number of luminous subhalos produced. We therefore investigate alterations to the reionization model and subsequent effects on our results in Section 5.

For that investigation, and for use in determining the radial distribution of satellites which survive reionization, we employ a simple model inspired by Lunnan et al. (2012) and Peter & Benson (2010). While exploring parameter space with detailed hydrodynamic or semi-analytic reionization models would be more rigorous, it is beyond the scope of this paper. For a halo to form stars by $z = 0$, it must either reach a critical size for H_2 cooling and atomic line cooling before reionization, or become massive enough after reionization to reaccrete and cool gas. We define the size thresholds in terms of v_{max} , calling them $v_{\text{max}}^{\text{pre}}$ and $v_{\text{max}}^{\text{filt}}$ respectively. Fixing reionization to happen instantaneously at $z = 13.3$, approximately the mean redshift in the model used in Barber et al. (2014), we conduct a parameter search to minimize the difference between the Barber et al. (2014) luminous frac-

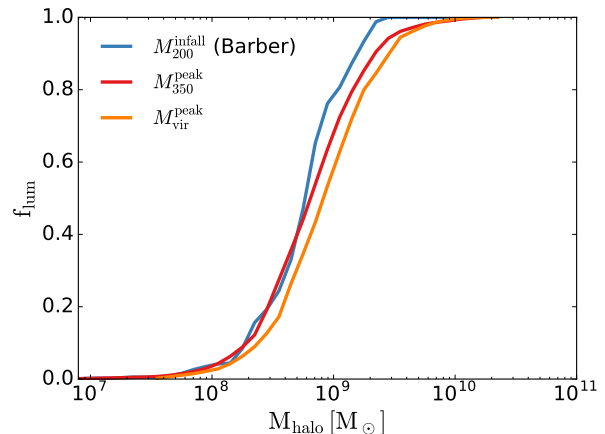


Figure 3. Fraction of dark matter halos that host luminous galaxies by $z = 0$ as a function of different mass definitions. The blue line is smoothed data from Barber et al. (2014), which uses a semi-analytic model applied to dark matter only simulations. The green and red lines are functions for alternate mass definitions, as inferred from the baseline reionization model and *Caterpillar* merger trees.

tion function of Fig. 3 and the one produced by applying the v_{max} cuts to the merger history in all *Caterpillar* simulations. We achieve a close fit ($< 4\%$ difference at any point) with $v_{\text{max}}^{\text{pre}} = 9.5$ and $v_{\text{max}}^{\text{filt}} = 23.5$ km/s.

Our value for $v_{\text{max}}^{\text{pre}}$ is consistent with expectations from the literature. While the threshold for H_2 cooling is more accurately weakly redshift dependent, it occurs around $M_{200} = 10^6 M_\odot$ or $T_{\text{vir}} = 2000 - 3000$ K (Tegmark et al. 1997; Madau et al. 2008; Power et al. 2014), corresponding to $4 - 7$ km/s at $z = 13.3$ in our simulations. Atomic line cooling occurs for larger mass halos, near $M_{200} = 10^8 M_\odot$ or $T_{\text{vir}} \approx 4000$ K (Bromm & Yoshida 2011), corresponding to $16 - 26$ km/s at $z = 13.3$ in our simulations. Halos which reach the atomic line cooling limit before reionization nearly universally form and retain stars by $z = 0$, whereas H_2 cooling minihalos may or may not retain stars due to reionization and supernova (Power et al. 2014). We thus expect $v_{\text{max}}^{\text{pre}}$ to lie between the minimum H_2 cooling threshold and the atomic cooling threshold, which it does. Moreover, it agrees closely with Okamoto & Frenk (2009) who inferred a value of $v_{\text{max}}^{\text{pre}} \approx 12$ km/s from hydrodynamic simulations where reionization occurs at $z = 8$. If we shift reionization to $z = 8$, our best fit value becomes 12.6 km/s.

Our value for $v_{\text{max}}^{\text{filt}}$ is consistent with the low end of expectations from the literature. This threshold for star formation to proceed after reionization has been termed the “filtering mass”, with initial values placed at $20 < v_{\text{max}} < 30$ km/s (Bovill & Ricotti 2009; Okamoto & Frenk 2009; Bovill & Ricotti 2011a,b). More recent publications have used higher values of $30 < v_{\text{max}} < 50$ km/s (Peter & Benson 2010; Lunnan et al. 2012; Garrison-Kimmel et al. 2014; Griffen et al. 2016a), highlighting uncertainty in how to model reionization.

2.4 Mass Functions and Monte Carlo Sampling

Using *Caterpillar*, we identify the mean SHMF for all isolated field galaxies and MW analogs. Since the AM models use different mass definitions for M_{halo} , we correspondingly find different SHMFs. In each case, the differential number of halos in a given mass interval, $\frac{dN}{dM_{\text{sub}}}$, follows the form

$$\frac{dN}{dM_{\text{sub}}} = K_0 \left(\frac{M_{\text{sub}}}{M_{\odot}} \right)^{-\alpha} \frac{M_{\text{host}}}{M_{\odot}} \quad (2)$$

as has been identified in several previous studies (Gao et al. 2004b; van den Bosch et al. 2005; Dooley et al. 2014). The best fit values of α and K_0 do depend weakly on the host halo mass range, but change negligibly within a one dex host mass interval. Since Milky Way-like hosts are more than one dex larger than field halos, we separately compute best fit values of α and K_0 for satellites of field halos and satellites of Milky Way-like hosts. These values are computed for each mass definition and shown in Table 1. The mass functions count all self-bound subhalos (excluding subhalos of subhalos) within R_{vir} at $z = 0$ regardless of the mass definition. M_{host} , however, uses the same mass definition as M_{sub} . We also considered a SHMF form where $\frac{dN}{dM_{\text{sub}}}$ is a power law function of $M_{\text{sub}}/M_{\text{host}}$ rather than being directly proportional to the host mass, but find the best fit parameters are more sensitive to the host halo mass range considered.

The mean number of dark matter subhalos, \bar{N} , around a host of mass M_{host} is found by integrating equation (2) from M_{min} to M_{host} to yield:

$$\bar{N} = \frac{K_0 M_{\text{host}}}{\alpha - 1} (M_{\text{min}}^{1-\alpha} - M_{\text{host}}^{1-\alpha}) \quad (3)$$

where M_{min} is a halo mass at which no star formation occurs in any model due to reionization. We choose a conservative value of $10^{7.4} M_{\odot}$. Since subhalo abundances are approximately Poisson distributed around the mean, we generate random realizations of the number of subhalos between M_{min} and M_{host} according to a Poisson distribution with a mean $\lambda = \bar{N}$, and then randomly assign halo masses to them according to the SHMF. More accurately, subhalo abundances follow a negative binomial distribution with the variance of \bar{N} increasing relative to that of a Poisson distribution as $M_{\text{sub}}/M_{\text{host}}$ decreases (Boylan-Kolchin et al. 2010; Mao et al. 2015; Lu et al. 2016). However, Boylan-Kolchin et al. (2010) find that the super Poissonian spread only becomes important for $M_{\text{sub}}/M_{\text{host}} \leq 10^{-3}$. Otherwise Poisson statistics remain a good approximation, as verified in the *Caterpillar* suite. The largest field halo we consider is $\sim 6 \times 10^{10} M_{\odot}$, and only subhalos with $M_{\text{vir}} \gtrsim 10^8 M_{\odot}$ contribute to satellites with $M_* > 10^3 M_{\odot}$, so the minimum ratio relevant to this study is $M_{\text{sub}}/M_{\text{host}} = 1.7 \times 10^{-3}$. In this instance, $\sigma_{\bar{N}}/\sigma_{\text{Poisson}} \leq 1.2$. For all other field halos and for abundances of more luminous satellites, our Poisson approximation is even more accurate.

Once halo masses are assigned, they are chosen to be luminous or dark with probabilities following the luminous fraction as a function of halo mass as shown in Fig. 3. The luminous halos are then assigned a stellar mass according to the $M_* - M_{\text{halo}}$ relationship and scatter (if any) of the model under consideration.

2.5 Inferring M_{halo} from M_*

Given a target host halo, its total virial mass is needed in order to generate a realization of its SHMF. However, the dark matter mass is essentially impossible to measure directly for Local Group field dwarfs. Lensing methods are not available, and the mapping between the dynamical mass within the half-light radius of the galaxy (with stellar kinematics) to the virial mass is highly dependent on the dark-matter density profile.

Instead, M_{halo} can be inferred from an AM model and the more easily measured total stellar mass. While $M_* - M_{\text{halo}}$ relationships give the median stellar mass for a fixed halo mass, by modeling the conditional probability function $P(M_* | M_{\text{halo}})$, taking the inverse of the function does not yield median halo masses when there is scatter in the relationship. In other words, $P(M_{\text{halo}} | M_*) \neq P(M_* | M_{\text{halo}})$, but $P(M_{\text{halo}} | M_*) \propto P(M_* | M_{\text{halo}}) P(M_{\text{halo}})$. A greater preponderance of lower mass halos which upscatter in stellar mass than higher mass halos which downscatter means the true median M_{halo} is less than that suggested by the AM relationship.

We compute the unnormalized $P(M_{\text{halo}} | M_*)$ in logarithmic intervals by multiplying the host halo mass function, $dn/d\log M$, by the fraction of halos that are luminous, and again by the likelihood of it hosting M_* given an AM model and Gaussian distributed scatter. For the mass functions, we use the form from Sheth & Tormen (2002) and use a transfer function from Eisenstein & Hu (1998). Given a fixed stellar mass, we assign relative probabilities to halo masses on a log-scale, then normalize the distribution and find the 50th percentile. This represents the median expected M_{halo} for a fixed M_* . Multiplying by the luminous fraction of galaxies makes a $< 1\%$ effect in all cases except for the GK16 model when $M_* < 6 \times 10^6 M_{\odot}$.

For the GK16 model, this results in halo masses that are 16 – 34% smaller than the value inferred by inverting the $M_* - M_{\text{halo}}$ relationship. For the GK14 model, the authors estimate a 0.2 dex lognormal scatter, which results in a 6 – 10% reduction. The Moster and Brook models do not mention any scatter, but for consistency we continue to assume a 0.2 dex scatter, yielding a 6 – 7% and 5 – 8% mass reduction respectively. While we assume a scatter to infer halo masses, we do not implement a scatter in assigning stellar mass to satellites in any model but GK16 since it is the only one which explicitly takes scatter into account when finding the best fit $M_* - M_{\text{halo}}$ function.

3 RESULTS

In the following subsections we compute the mean expected number of luminous satellite galaxies, \bar{N}_{lum} , above a given stellar mass threshold, M_*^{thresh} , and the probability of at least one satellite existing above M_*^{thresh} as a function the host galaxy’s stellar mass. For the rest of the paper, we consider galaxy stellar masses above $M_* > 10^3 M_{\odot}$, since smaller “hyperfaint” galaxies have so few stars that they will be difficult to detect above the background. All values are found using the methodology presented in Section 2, generating 30000 random realizations of satellite populations per host. Due to uncertainty in mass to light ratios, we strictly report on stellar mass, not stellar luminosity.

Table 1. Subhalo mass functions for MW size halos and dwarf field halos

Mass Definition	α (field)	K_0 (field)	α (MW analog)	K_0 (MW analog)	AM Model(s)
M_{200}^{infall}	1.81	0.000635	1.84	0.000854	Moster
$M_{\text{vir}}^{\text{peak}}$	1.82	0.000892	1.87	0.00188	GK14, GK16, Behroozi
M_{350}^{peak}	1.81	0.000765	1.87	0.00200	Brook

Note. — Values of α and K_0 in equation (2) for the mean subhalo mass function for various definitions of subhalo mass. Columns two and three designate values for isolated dwarf field galaxies, and four and five for Milky Way analogs. The parameters of the mass function are approximately independent of host halo mass over a one dex interval. Milky Way analogs and field dwarf halos need to be separated, but within each category one set of parameters is sufficient. The abundance matching models employing each definition are indicated.

3.1 Validation of our models with the Milky Way satellite system

To verify our model implementations, we predict the number of satellites around a Milky Way-sized galaxy. We fix the host’s dark matter mass to $M_{\text{vir}} = 1.4 \times 10^{12} M_{\odot}$ and plot the mean number of satellites as a function of M_*^{thresh} in the upper panel of Fig. 4. We include predictions of each abundance-matching model with and without reionization to indicate how much reionization suppresses the formation of low mass galaxies. The abundances are all scaled to a radius of 300 kpc using Eq. (4) (presented later in Section 4) since that distance corresponds to published completeness limits for satellite surveys of the Milky Way (Walsh et al. 2009; Drlica-Wagner et al. 2015). The models are all consistent with the high-mass end of the MW satellite stellar mass function. There are 11 MW satellites with $M_* > 4.5 \times 10^5 M_{\odot}$ within 300 kpc of the Galactic Center (Garrison-Kimmel et al. 2016); all models are consistent with 11 such satellites within 1σ Poisson errors. Since no model was calibrated exclusively to the MW satellites, and there is uncertainty in the mass of the Milky Way from $\approx 0.5 - 2.5 \times 10^{12} M_{\odot}$ (Wang et al. 2015), an exact agreement with the MW luminosity function is not expected. For instance, while the Brook model is consistent with Milky Way classical dwarf satellite counts for the fiducial MW halo mass, the model would better match the MW system with a higher assumed mass.

On the faint end, the models predict a median of 66, 71, 67, and 37 satellites with $M_* > 10^3 M_{\odot}$ for the Moster, GK14, GK16, and Brook models respectively. The first three models are in strong agreement with a prediction by Hargis et al. (2014), who estimated 69 satellites above $10^3 L_{\odot}$ in the MW out to 300 kpc from observations and completeness limits. Drlica-Wagner et al. (2015) also make a consistent prediction of 70 UFDs in the MW when excluding the sub-substructure of UFDs in the Large and Small Magellanic Clouds.

If ≥ 70 UFDs, or more than 80 satellites with $M_* > 10^3 M_{\odot}$ in total are discovered in the MW in the future, it would strongly disfavor the Brook model as implemented. It is difficult to reconcile the Brook model even if the MW halo is on the massive side. At a MW mass of $2 \times 10^{12} M_{\odot}$, the Brook model predicts 53 satellites, more than 2σ less than 80

where σ is taken from the negative binomial distribution in (Boylan-Kolchin et al. 2010). If reionization was shut off entirely, the predicted number of satellites in the Brook model could increase by 20%. A more likely maximal increase of 10% would still mean the model predicts the MW has an unusually high number of UFDs for its size. The rarity of LMC and SMC sized systems in a MW-like halo (Boylan-Kolchin et al. 2010; Busha et al. 2011), though, could be evidence in favor of that argument.

In stark contrast, reionization has a large impact on the Moster, GK14, and GK16 models. In these models it is absolutely necessary to include reionization or else an additional 110 to 205 luminous satellites with $M_* > 10^3 M_{\odot}$ would be predicted. Based on the MW comparison, we expect numbers predicted by the Brook model to be on the low end of possibilities for satellites of dwarf galaxies, and values from the other models to be closer to median expectations.

3.2 How many satellites of dwarfs are there?

In the lower panel of Fig. 4 we again show the satellite abundance as a function of minimum M_*^{sat} , but now fix the host halo stellar mass to $M_* = 2.7 \times 10^8 M_{\odot}$ to reflect the largest field dwarf galaxy, IC 5152. Without a direct measurement of total baryonic plus dark matter mass available, we convert from stellar mass to halo mass for each AM model as described in Section 2.5. The radius out to which subhalos are counted is the R_{vir} associated with the halo’s total mass, unlike in the top panel. Whereas the Moster, GK14, and GK16 models make similar predictions when the host’s total mass is fixed, as in the upper panel, their predictions diverge when instead the host’s stellar mass is fixed, as in the lower panel. This is due to the GK models having a lower $M_* - M_{\text{halo}}$ relationship in the range of field halos, which leads to predicting more massive halos for fixed stellar mass. Furthermore, the GK16 and GK14 models are separated due to the larger scatter in the GK16 model, which leads to the GK16 model preferring smaller host halo masses than does the GK14 model. The models predict a mean of $\sim 2 - 6$ satellites with M_* above $10^3 M_{\odot}$, $\sim 1 - 4$ above $10^4 M_{\odot}$, and $\sim 1 - 2$ above $10^5 M_{\odot}$ for a galaxy like IC 5152.

In Fig. 5, we show the dependence of satellite abundances on the host galaxy’s size in terms of its stellar mass. The top panel plots the median number of satellites with

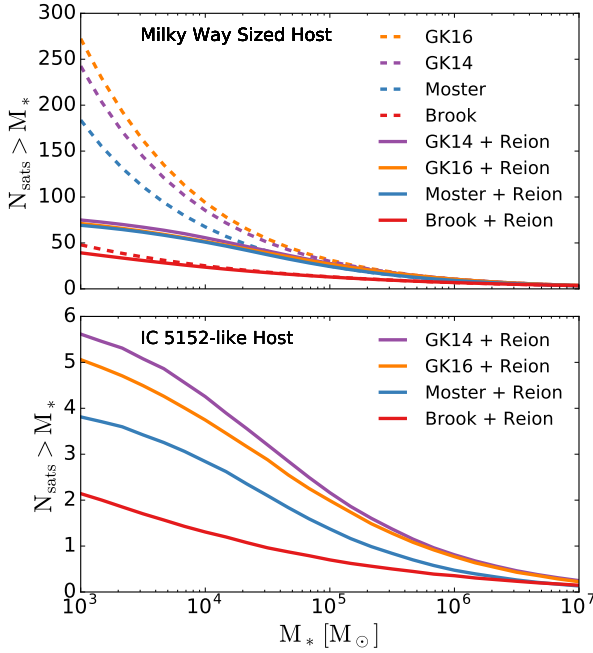


Figure 4. Upper Panel: Mean number of satellites around a MW-sized host with total mass $1.4 \times 10^{12} M_{\odot}$ as a function of satellite stellar mass. While the Moster, GK14, and GK16 models predict similar numbers of satellites after accounting for reionization, the Brook model predicts significantly fewer. Due to its steep M_* – M_{halo} relationship, the Brook model is also minimally affected by reionization whereas the other models are reduced by more than 60% on the low mass end. Lower Panel: Mean number of satellites around a host of $M_* = 2.7 \times 10^8 M_{\odot}$, approximately that of IC 5152, as a function of satellite stellar mass. While the Moster, GK14, and GK16 models make similar predictions if the host’s total mass is fixed, they predict different abundances when stellar mass is fixed.

$M_*^{\text{sat}} > 10^3 M_{\odot}$, the middle panel with $M_*^{\text{sat}} > 10^4 M_{\odot}$, and the bottom panel with $M_*^{\text{sat}} > 10^5 M_{\odot}$. The dashed vertical lines correspond to the stellar masses of the five largest known field galaxies in the Local Group, IC 5152, IC 4662, IC1613, NGC 6822, and NGC 3109. For IC 5152 for instance, the models predict a mean of 1.3 satellites with $M_* > 10^4 M_{\odot}$ on the low end in the Brook model, to 4.3 satellites in the GK14 model.

This figure shows that the number of expected UFDs is a strong function of stellar mass of the host. Below a host stellar mass of $10^7 M_{\odot}$, there is a mean of less than one UFD sized satellite according to all models, indicating many hosts will have no satellites above $10^3 M_{\odot}$. For a host of $10^8 M_{\odot}$ and larger, at least one satellite per host is expected.

A list of known isolated field galaxies and the mean number satellites within their virial volume is listed in Table 2. Galaxies and stellar masses were compiled from [McConnachie \(2012\)](#), and supplemented with values from [Karachentsev et al. \(2014\)](#), [McQuinn et al. \(2015\)](#), and [Karachentsev et al. \(2015\)](#) for KK 258, Leo P, and KKs 3

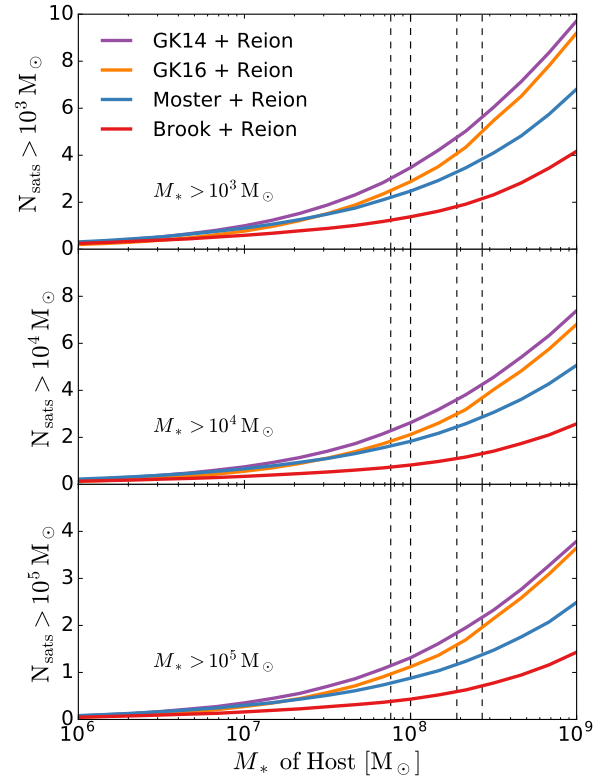


Figure 5. Mean number of satellites with stellar mass above $10^3 M_{\odot}$ (upper panel), $10^4 M_{\odot}$ (middle panel), and $10^5 M_{\odot}$ (lower panel) as a function of a host halo’s total stellar mass, M_* . Each abundance matching model predicts different values, but all agree that satellites should exist around hosts with $M_* \geq 10^8 M_{\odot}$. Vertical lines correspond to the stellar masses of the five field galaxies listed in Table 2 with the largest stellar masses

respectively. We give an indication of the probabilistic distribution of satellites by including the 20th and 80th percentile of abundance, and the probability that at least one satellite exists, $P(\geq 1)$.

Table 2. Mean number of satellites with $M_* > 10^4 M_\odot$ around Local Group dwarf field galaxies

Name	M_* [$10^6 M_\odot$]	Moster			GK14			GK16			Brook		
		\bar{N}_{lum}	20/80%	$P(\geq 1)$	\bar{N}_{lum}	20/80%	$P(\geq 1)$	\bar{N}_{lum}	20/80%	$P(\geq 1)$	\bar{N}_{lum}	20/80%	$P(\geq 1)$
Leo T	0.14	0.08	0/0	0.07	0.05	0/0	0.05	0.03	0/0	0.04	0.05	0/0	0.05
And XXVIII	0.21	0.10	0/0	0.09	0.07	0/0	0.07	0.05	0/0	0.05	0.06	0/0	0.06
KKR 3	0.54	0.16	0/0	0.15	0.13	0/0	0.12	0.09	0/0	0.09	0.10	0/0	0.10
Tucana	0.56	0.17	0/0	0.15	0.13	0/0	0.12	0.09	0/0	0.09	0.10	0/0	0.09
Leo P	0.56	0.17	0/0	0.15	0.13	0/0	0.12	0.09	0/0	0.09	0.10	0/0	0.10
And XVIII	0.63	0.17	0/0	0.16	0.15	0/0	0.13	0.10	0/0	0.09	0.11	0/0	0.10
Phoenix	0.77	0.19	0/0	0.18	0.17	0/0	0.15	0.11	0/0	0.11	0.12	0/0	0.11
KKH 86	0.82	0.19	0/0	0.18	0.17	0/0	0.15	0.12	0/0	0.11	0.12	0/0	0.11
Antlia	1.3	0.25	0/1	0.22	0.23	0/1	0.20	0.16	0/0	0.15	0.15	0/0	0.14
KKR 25	1.4	0.26	0/1	0.23	0.24	0/1	0.21	0.16	0/0	0.15	0.15	0/0	0.14
Aquarius	1.6	0.28	0/1	0.24	0.26	0/1	0.22	0.18	0/0	0.16	0.16	0/0	0.15
DDO 113	2.1	0.32	0/1	0.27	0.30	0/1	0.26	0.21	0/0	0.19	0.18	0/0	0.17
Cetus	2.6	0.35	0/1	0.29	0.35	0/1	0.29	0.24	0/1	0.21	0.20	0/0	0.18
ESO 294-G010	2.7	0.36	0/1	0.30	0.35	0/1	0.29	0.25	0/1	0.22	0.21	0/0	0.18
Sagittarius dIrr	3.5	0.41	0/1	0.33	0.41	0/1	0.34	0.30	0/1	0.25	0.23	0/1	0.20
ESO 410-G005	3.5	0.41	0/1	0.33	0.41	0/1	0.34	0.29	0/1	0.25	0.23	0/1	0.21
KKH 98	4.5	0.46	0/1	0.37	0.48	0/1	0.38	0.35	0/1	0.29	0.25	0/1	0.22
Leo A	6	0.52	0/1	0.41	0.56	0/1	0.43	0.41	0/1	0.33	0.28	0/1	0.25
GR 8	6.4	0.54	0/1	0.41	0.58	0/1	0.44	0.43	0/1	0.34	0.29	0/1	0.25
Pegasus dIrr	6.6	0.54	0/1	0.42	0.59	0/1	0.45	0.43	0/1	0.35	0.29	0/1	0.25
UGC 9128	7.8	0.59	0/1	0.45	0.65	0/1	0.47	0.48	0/1	0.38	0.31	0/1	0.27
UGC 4879	8.3	0.60	0/1	0.46	0.67	0/1	0.49	0.49	0/1	0.39	0.32	0/1	0.27
KK 258	14	0.77	0/1	0.53	0.90	0/2	0.59	0.67	0/1	0.49	0.39	0/1	0.32
UGCA 86	16	0.82	0/1	0.56	0.97	0/2	0.62	0.74	0/1	0.53	0.41	0/1	0.33

Table 2 – *continued* Mean number of satellites with $M_* > 10^4 M_\odot$ around Local Group dwarf field galaxies

Name	M_* [$10^6 M_\odot$]	Moster			GK14			GK16			Brook		
		\bar{N}_{lum}	20/80%	$P(\geq 1)$	\bar{N}_{lum}	20/80%	$P(\geq 1)$	\bar{N}_{lum}	20/80%	$P(\geq 1)$	\bar{N}_{lum}	20/80%	$P(\geq 1)$
DDO 99	16	0.82	0/1	0.56	0.98	0/2	0.62	0.73	0/1	0.52	0.41	0/1	0.34
UKS 2323-326	17	0.84	0/2	0.57	1.01	0/2	0.63	0.76	0/1	0.54	0.41	0/1	0.34
UGC 8508	19	0.88	0/2	0.58	1.07	0/2	0.66	0.82	0/1	0.56	0.43	0/1	0.35
KKs 3	23	0.96	0/2	0.62	1.19	0/2	0.69	0.92	0/2	0.60	0.47	0/1	0.37
NGC 4163	37	1.19	0/2	0.70	1.53	0/3	0.78	1.22	0/2	0.70	0.55	0/1	0.42
WLM	43	1.28	0/2	0.72	1.67	1/3	0.81	1.34	0/2	0.74	0.59	0/1	0.44
Sextans A	44	1.28	0/2	0.72	1.70	1/3	0.82	1.34	0/2	0.74	0.60	0/1	0.45
DDO 125	47	1.32	0/2	0.74	1.75	1/3	0.83	1.40	0/2	0.76	0.61	0/1	0.46
DDO 190	51	1.37	0/2	0.74	1.84	1/3	0.84	1.47	0/2	0.77	0.62	0/1	0.47
Sextans B	52	1.37	0/2	0.75	1.85	1/3	0.84	1.48	0/2	0.78	0.64	0/1	0.47
IC 3104	62	1.50	0/2	0.77	2.04	1/3	0.87	1.64	1/3	0.81	0.68	0/1	0.49
NGC 3109	76	1.63	1/3	0.80	2.26	1/3	0.90	1.81	1/3	0.84	0.73	0/1	0.52
NGC 6822	100	1.84	1/3	0.84	2.62	1/4	0.93	2.12	1/3	0.88	0.83	0/2	0.56
IC 1613	100	1.84	1/3	0.84	2.62	1/4	0.93	2.12	1/3	0.88	0.83	0/2	0.56
IC 4662	190	2.44	1/4	0.91	3.61	2/5	0.97	2.99	1/4	0.95	1.09	0/2	0.67
IC 5152	270	2.83	1/4	0.94	4.25	2/6	0.98	3.73	2/5	0.98	1.30	0/2	0.73

Note. — Mean number of satellites with $M_* > 10^4 M_\odot$ expected to exist within the virial volume of known Local Group dwarf irregular and dwarf spheroidal galaxies as predicted with various AM models. The 20th and 80th percentile of the satellite abundance distributions are included in the second column. Also shown is the probability of finding at least one satellite around each galaxy, $P(\geq 1)$.

3.3 Likelihood of finding at least one satellite

Another important metric in determining the merit of searching for satellites of field dwarf galaxies is the probability that at least one satellite exists around a host. In Fig. 6 we show the probability that at least one satellite with $M_*^{\text{sat}} > 10^3, 10^4$ and $10^5 M_\odot$ exists around a host as a function of M_* of the host. Dotted vertical lines again show the stellar masses of the five largest known field galaxies in the Local Group. For the largest field galaxy, IC 5152, the probability of a satellite with $M_*^{\text{sat}} > 10^4 M_\odot$ is $> 90\%$ according to the Moster, GK14, and GK16 models. It drops to 73% for the Brook model. For the 5th largest field galaxy, the probability remains above 80% in the first three models, and is 51% for the Brook model.

The high likelihoods indicate that a comprehensive search of Local Group dwarf galaxies is likely to yield at least one new satellite discovery, even if only the five most massive field dwarfs are surveyed. For the Moster, GK14, and GK16 models, the probability of one satellite with $M_* > 10^5 M_\odot$ is $> 99\%$ if all five of the largest field galaxies are surveyed to their full virial volume. We choose to highlight the five largest because of this fact. In the Brook model, the probability is 92%, but goes to $> 99\%$ for $M_* > 10^4 M_\odot$.

In Fig. 7, we show a probability distribution function for the total number of satellites expected around these five largest field galaxies. The three panels show values for abundances above stellar mass thresholds of $10^3, 10^4$, and $10^5 M_\odot$. When comparing to Fig. 8, which shows the same distribution except for all 38 field dwarfs listed in Table 2, we demonstrate that surveying just the five largest galaxies would reveal $\sim 1/3$ of the total population of satellites of field dwarfs.

The shape of the distributions is driven mostly by Poisson statistics in the number of dark matter subhalos. The randomness of reionization suppressing star formation contributes a smaller additional component. In the case of the Moster model, there is another perturbation due to differing halo infall times, and in the case of the GK16 model, from scatter in $M_* - M_{\text{halo}}$. The combined uncertainty arising from counting statistics and abundance matching models results in a broad distribution of possible satellite tallies. The distinct curves from each abundance matching model, in particular comparing the Brook and GK14 models, indicates how observing satellites could provide important insight into ruling out or improving AM models. This is particularly true for satellites above $10^5 M_\odot$ since reionization has little effect on the number of satellites above that threshold, and those satellites are easier to discover. Probing down to satellites near $10^3 M_\odot$ or $10^4 M_\odot$ would help constrain the effects reionization when compared with the number of satellites found above $10^5 M_\odot$, but would be observationally more challenging.

4 SURVEY STRATEGY: DEPENDENCE ON FIELD OF VIEW

Due to the geometry of a line of sight, the values we report in Section 3 for the number of satellites within a virial volume do not directly translate into expectations for an observed field of view. For instance, the number of dwarfs-of-dwarfs

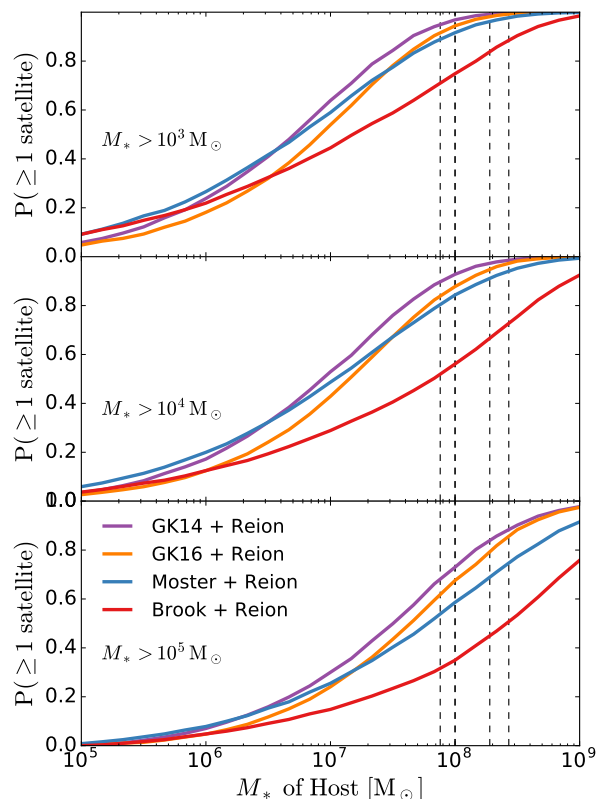


Figure 6. Probability that at least one satellite with stellar mass above $10^3 M_\odot$ (upper panel), $10^4 M_\odot$ (middle panel), or $10^5 M_\odot$ (lower panel) exists around a host with stellar mass M_* . The Moster, GK14, and GK16 models all predict a high likelihood of at least one satellite with $M_* > 10^4 M_\odot$ existing around each of the five largest field galaxies, whose stellar masses are indicated by dotted lines (and listed in Table 2). The Brook model predicts lower probabilities, but still $> 50\%$ for each of these galaxies.

that may exist in the Solo survey depends on their field of view, the distance to target galaxies, the radius of target galaxies, and the radial distribution of satellites within a galaxy. Future campaigns must account for these details when designing a strategy for limited amounts of telescope time. Both targeting larger mass host galaxies and focusing on the innermost region will increase the projected density of satellites. If the observing goal is to discover as many as possible, would it be better to observe the inner region of a lower mass host, or the outer regions of a higher mass host? We address this issue in detail by making predictions specifically for the Solo survey, and discussing a survey strategy.

We begin by computing a scaling factor to convert the predicted values of the mean number of luminous satellites within a host's virial radius to values expected from surveying circular apertures centered on a host. As found in Han et al. (2016) and confirmed in our simulation suite, satellites are distributed approximately spherically symmetrically around a host and the normalized distribution does

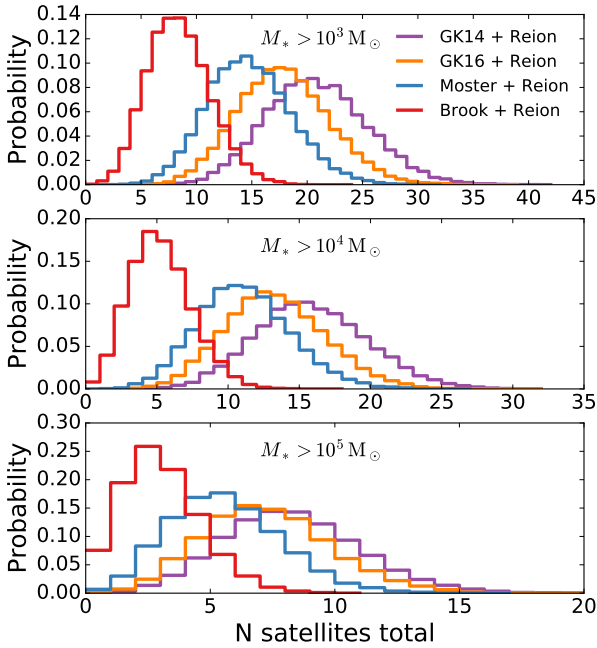


Figure 7. Probability distribution for the total number of satellites expected to be found with $M_* > 10^3, 10^4$ and $10^5 M_\odot$ around the combined largest five Local Group field galaxies. The GK14 and GK16 models predict over twice the number of satellites as the Brook model, whose predictions are on the lowest end possible to be consistent with MW satellites, and thus are likely a lower limit to the number of satellites of dwarf galaxies. According to the Moster, GK14 and GK16 models, there is a $> 99\%$ that at least one satellite with $M_* > 10^5 M_\odot$ exists. These five largest galaxies contain $\sim 1/3$ of the total number of satellites of field dwarfs.

not vary with host halo size. This allows us to express the normalized cumulative abundance of satellites generically around a host as $K(r)$. We compute $K(r)$ from the subhalos which are deemed luminous in our reionization model across all 33 *Caterpillar* simulations at $z = 0$. Selecting only luminous satellites is crucial, because they are more centrally concentrated than the full sample of dark matter subhalos, as previously found and discussed in Gao et al. (2004a), Starkenburg et al. (2013), Barber et al. (2014), and Sawala et al. (2016).

The distribution of all dark matter subhalos and the subset of luminous satellites is plotted in Fig. 9. For comparison, we also plot the cumulative distribution of known MW satellites with stellar mass above the observed completeness limit of $M_* = 2 \times 10^5 M_\odot$ that are within 300 kpc of the Galactic Center. We exclude the LMC and SMC since they occur rarely in MW-sized galaxies (Boylan-Kolchin et al. 2010; Busha et al. 2011) and they are spatially correlated. The positions and stellar masses of satellites were taken from McConnachie (2012),¹ Our predicted radial distribution of

¹ Available online at http://www.astro.uvic.ca/~alan/Nearby_Dwarf_Database.html.

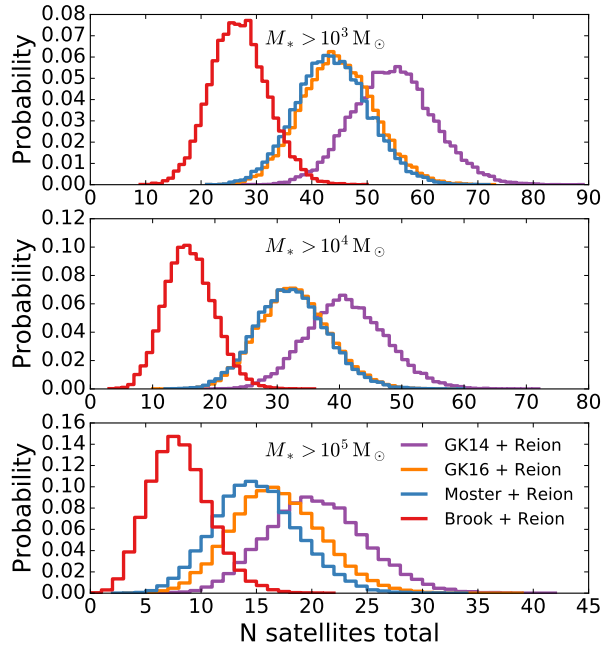


Figure 8. Probability distribution for the total number of satellites expected to be found with $M_* > 10^3, 10^4$ and $10^5 M_\odot$ around all Local Group field galaxies listed in Table 2. There is an even greater separation of the Brook and GK14 models than in Fig. 7. Also in comparison, the GK16 model makes predictions more similar to the Moster model due to a greater scatter in M_* for the lower mass halos causing the median predicted M_{halo} to be less for a given halo stellar mass.

satellite galaxies fits remarkably well to the MW satellites. In contrast, the distribution inferred from all dark matter subhalos does not, demonstrating the importance of subhalo selection effects due to reionization.

For ease of use, we find a very tight match to the data with a piecewise analytic function. It takes the form

$$K(R) = \begin{cases} k_1 R + k_2 R^2 + k_3 R^3 & R < 0.2 \\ k_4 \arctan\left(\frac{R}{k_5} - k_6\right) & 0.2 \leq R \leq 1.5 \end{cases} \quad (4)$$

with best fit values of the constants $k_1 = -0.2615$, $k_2 = 6.888$, $k_3 = -7.035$, $k_4 = 0.9667$, $k_5 = 0.5298$, and $k_6 = 0.2055$. We find that luminous satellites with a lower peak mass are slightly more centrally concentrated than more massive luminous satellites since they are subject to greater selection effects from reionization. However, the shift in $K(R)$ is $\lesssim 10\%$ which is small compared to Poisson noise and much smaller than the difference between all subhalos and only luminous subhalos. Since galaxies are self-similar, and the radial distribution varies only weakly with satellite mass range, it is possible to simply multiply $K(R)$ by the expected number of satellites in any mass interval within the virial radius of a host (taken from Fig. 5 for instance) to yield the number of satellites within a radius r/R_{vir} .

By integrating the density function $\frac{1}{4\pi r^2} \frac{dK}{dr}$ over a cylinder of radius $R \equiv r/R_{\text{vir}}$ and half depth $Z \equiv z/R_{\text{vir}}$ where r and z are cylindrical coordinates centered on the host galaxy,

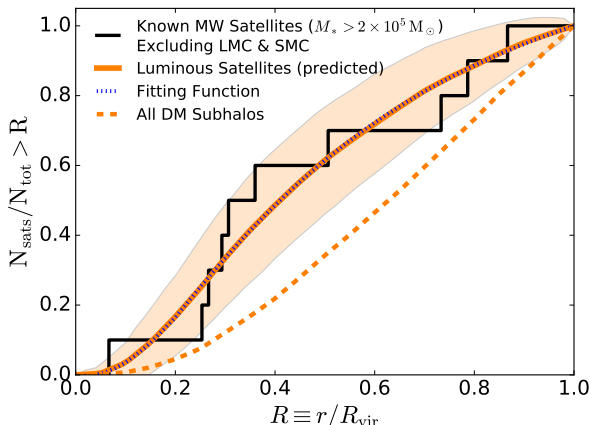


Figure 9. Normalized radial distribution of satellites scaled to a host with $R_{\text{vir}} = 300$ kpc. The radial distribution of satellites which survive reionization in our simulations (and are thus luminous) agree well with the radial distribution of known MW satellites, whereas the radial distribution of all dark matter subhalos does not. The sample of known MW satellites includes all satellites with stellar mass above the completeness limit of $M_* = 2 \times 10^5 M_\odot$, except for the LMC and SMC which are known to be spatially correlated and very rare. One sigma variation about the prediction for luminous satellites is shown with a shaded band. It is important to take reionization into account when predicting the radial distribution of satellites, and to not assume it follows the distribution of all dark matter subhalos. A fitting function for the predicted radial distribution is given by equation (4) and plotted with a dotted line.

one gets the number of satellites expected in a line of sight relative to the number within R_{vir} . We call this quantity $K_{\text{los}}(R)$. We numerically integrate the function and show the result in Fig. 10, fixing Z to a value of 1, approximately where halos are likely to be bound to the host halo, and 1.5. $Z = 1.5$ encompasses the “splashback” radius for slowly accreting halos, defined as the distance to first apocenter of orbiting bound satellites (More et al. 2015). It also represents a distance beyond which the density of additional satellites diminishes rapidly towards zero. Since galaxies at all values of z are in the line of sight, $Z = 1.5$ is a more accurate reflection of what satellites can be observed.

There are several important results from this exercise. First, if one were to search out to the projected virial radius of the host, one would find $\sim 10\%$ more dwarfs than one would expect based on the number of dwarfs strictly within the spherical virial volume. This comes from dwarfs inhabiting a region outside the virial radius that can be imagined by circumscribing a sphere by a cylinder, and then extending the depth (height) of the cylinder to the splashback radius. Second, the number of expected dwarfs rises sublinearly with aperture radius for $R > 0.5$, regardless of the depth of the line-of-sight, Z , under consideration. This is in contrast to the survey area, which grows as the square of the aperture radius. Therefore, in the absence of increased backgrounds like an extended stellar halo, which is unlikely to be significant for dwarfs (Pillepich et al. 2014), pointings centered on

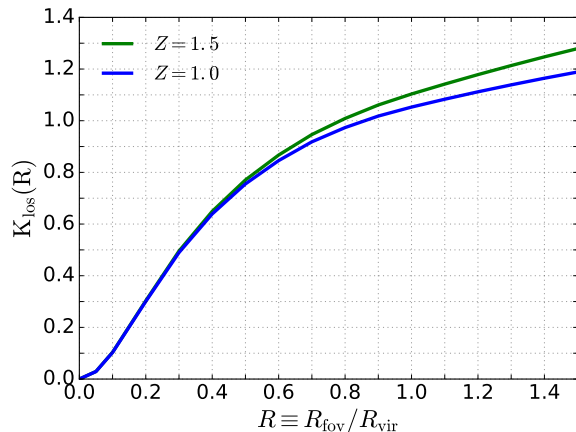


Figure 10. Multiplicative value used to scale the expected number of satellites within a halo’s virial radius to the expected number of satellites within an observed column whose field of view has the radius R_{fov} on the sky at the distance of the target host galaxy. The column is centered on the galactic center and has a depth of $2 \times Z \equiv 2 \times z/R_{\text{vir}}$. A value of $Z = 1$ means the center of the column extends from the near edge of the virial radius to the far edge. For instance, observing a field of view that has $R = 1/2$, $Z = 1$ corresponds to a multiplicative factor of 0.76.

the host galaxy will have higher satellite yields than individual pointings in the outskirts of the host halos.

In light of this, the most efficient strategy for finding dwarf-of-dwarf satellites is to first target the innermost region of the most massive dwarf hosts. Additional observations should map out the whole virial volume of the biggest dwarfs before targeting down the field dwarf stellar mass function, unless environment is a strong motivating factor in the dwarf-of-dwarf search.

What is the transition between a “big” and a “small” dwarf host? The optimal transition point from searching the innermost region of smaller galaxies to the whole volume of larger galaxies depends on which galaxies are targeted and the telescope’s field of view. It can be calculated from Fig. 10 and Table 3. Similar to $K(R)$, $K_{\text{los}}(R, Z)$ can be multiplied by the number of satellite galaxies within the virial radius of any host, for any satellite mass interval, to yield the number of satellites within a specified line of sight. Table 3 lists the distances to all isolated field galaxies, repeats the mean number of galaxies within the virial radius, \bar{N}_{lum} , for convenience, and lists the virial radius of each galaxy inferred from the AM models. R_{vir} refers to the Bryan & Norman (1998) definition, consistent with the radius used to determine all SHMFs. We infer M_{halo} from the AM model and host halo’s stellar mass, then convert M_{halo} to M_{vir} assuming an NFW halo density profile, and finally find R_{vir} from M_{vir} .

As an example of computing the number of galaxies in a field of view, IC 5152 is located at a distance of 1.7 Mpc (Zijlstra & Minniti 1999). DECam has a 2.2° field of view, resulting in a 33 kpc observed radius. At a Moster-model-estimated total halo mass of $5.2 \times 10^{10} M_\odot$, IC 5152 has a virial radius of 101 kpc. Using Fig. 10 with $Z = 1.5$, the number of satellites reported for the virial volume is multiplied by 0.54 to yield 1.5 expected satellites in the line of sight.

An equivalent calculation for the GK16 model produces 1.8 expected satellites, 2.0 for the GK14 model, and 0.7 for the Brook model. If we were to survey the whole virial volume of IC 5152, we would require an additional 8 distinct pointings, and would expect to find only 1 – 2 more satellites. This example also demonstrates that part of the disparity between the Moster, GK14, and GK16 models is generated from predicting different virial volumes for a host with fixed stellar mass. When normalizing to more equivalent volumes, as exemplified here, their predictions start converging.

We apply the same calculations to all of the galaxies in Table 3 using an approximate field of view from the Solo dwarf survey. Solo has a $1^\circ \times 1^\circ$ camera (Higgs et al. 2016), which we approximate as a circular aperture with radius 0.56° . We present all of the values expected for Solo in the \bar{N}_{fov} column. Our table contains all but two of the galaxies they target, Perseus and HIZSS3A(B), for which we could not obtain stellar masses. Due to a small field of view, nearly all galaxies have a mean expected number of satellites of fewer than 1. However, enough galaxies were surveyed that in aggregate multiple satellites with $M_* > 10^4 M_\odot$ could be in their observations.

5 SYSTEMATIC UNCERTAINTIES

Here we determine what the largest sources of uncertainty are for our luminous dwarf-of-dwarf number count predictions. We show some of them in Fig. 7: differences between AM models, counting statistics, and halo-to-halo variations. However, there are other sources of uncertainty that we quantify in this section. We introduce \bar{N}_{lum}^5 which is the mean total number of satellites with $M_* > 10^4 M_\odot$ that exist around the five largest field galaxies according to the Moster model. Using \bar{N}_{lum}^5 as a baseline, the GK14 model predicts 45% more satellites than the Moster model, and the Brook model predicts 55% less. Statistical fluctuations, driven mostly by Poisson noise, contribute a standard deviation of $\pm 30\%$. Not accounted for are systematic uncertainties in the stellar mass of the host, the total mass of the host, the SHMF, the infall time distribution for the Moster model, the magnitude of scatter in $M_* - M_{\text{halo}}$ for the GK16 model, and the reionization model used. Each of these uncertainties must be estimated before a robust prediction can be made regarding whether or not satellites of dwarfs could be discovered, and how many. We therefore estimate typical uncertainties in each input variable and the resultant effect of uncertainty on \bar{N}_{lum}^5 . Finally, we compare which uncertainties contribute most.

Table 4 lists each input variable and variation along with the corresponding % change in \bar{N}_{lum}^5 . The first value reports the % change in the number of satellites with $M_* > 10^4 M_\odot$, and the second value in parenthesis is for $M_* > 10^3 M_\odot$. When considering scatter in $M_* - M_{\text{halo}}$, \bar{N}_{lum}^5 refers to the GK16 model, otherwise all instances refer to the Moster model.

Uncertainty in the total halo mass, $M_{\text{halo}}^{\text{host}}$, is computed from the likelihood distribution for M_{halo} given M_* as described in Section 2.5. For the Moster model, one σ uncertainty in the largest field dwarf is +22% and –18%. Uncertainty in the GK14 and Brook models is similar, but in the GK16 model which has higher scatter in $M_* - M_{\text{halo}}$, one σ

is +28% and –35%. Consistent with \bar{N} being directly proportional to $M_{\text{halo}}^{\text{host}}$ to first order, as written in equation (3), a 22% change in halo mass results in a 23% change in \bar{N}_{lum}^5 .

For stellar mass, we choose an uncertainty of 25%, representative of the uncertainty ranges presented in Roediger & Courteau (2015). Due to the steep dependence of M_* on M_{halo} in the AM models, a change in M_* results in a smaller per cent change in the inferred M_{halo} . As a result, a 25% change in M_* yields just a 10–12% change in \bar{N}_{lum}^5 , whereas the same change in $M_{\text{halo}}^{\text{host}}$ yields a 26% change.

To estimate uncertainty in the infall times of satellites and the SHMF of field halos, we use a jackknife method with one simulation removed at a time. We find the mean infall time of satellites counting back from $z = 0$ to be $t_{\text{infall}} = 7.45 \pm 0.23$ Gyr for the field halos. Shifting the entire infall time distribution by 0.23 Gyr results in a negligible $< 1\%$ effect on \bar{N}_{lum}^5 . For the SHMF, $\alpha = 1.81 \pm 0.065$. We therefore adjust α to 1.88 and 1.75 and find the best fit value of K_0 for each slope. A steeper slope reduces M_* at the low M_{halo} end, causing fewer expected luminous satellites. A shallower slope does the opposite, with a total uncertainty of $\sim \pm 11\%$.

Next, we change the level of scatter in the GK16 model. A value of $\gamma = 0$ produces a constant lognormal scatter about $M_* - M_{\text{halo}}$ of $\sigma_{\text{scat}} = 0.2$ dex. Increasing γ to –0.5 increases the level of scatter relative to our baseline of $\gamma = -0.2$. Three different effects influence the overall outcome of modifying scatter. First, increasing scatter leads to smaller inferred halo mass for a fixed stellar mass, and thus fewer satellites. Second, in GK16’s model, increasing scatter requires a steeper $M_* - M_{\text{halo}}$ slope, which reduces M_* for a fixed M_{halo} , which subsequently reduces our predicted \bar{N}_{lum} . Third, increasing scatter causes more of the more numerous lower mass halos to upscatter above a detection threshold than higher mass halos to downscatter, which increases \bar{N}_{lum} . However, this third effect diminishes on the mass scale where reionization suppresses low mass galaxies. The interplay of all three effects is complex and model dependent, but ultimately results in less change to \bar{N}_{lum}^5 than exists between abundance matching models.

Lastly, we consider modifications to reionization. Using the model presented in Section 2.3, we are able to adjust the redshift of reionization to $z = 14.3, 11.3$, and 9.3 and catalog how \bar{N}_{lum}^5 responds in Table 4. We additionally adjust both v_{max} thresholds ($v_{\text{max}}^{\text{pre}}$ and $v_{\text{max}}^{\text{filt}}$) up by 25%, both of which create more dark halos, and down by 25%, both of which create more luminous halos.

Modifications to reionization can have enormous implications for the abundance of UFD satellites, but little effect on larger satellites. For instance, shifting reionization to later times, $z = 9.3$, increases \bar{N}_{lum}^5 by 65% for $M_* > 10^3 M_\odot$. For $M_* > 10^4 M_\odot$, it increases it by 20%, and for $M_* > 10^5 M_\odot$ there is only a 1% level effect. The same trends are true for adjusting $v_{\text{max}}^{\text{pre}}$ and $v_{\text{max}}^{\text{filt}}$. For $M_* > 10^3 M_\odot$ there can be as high as a 70% increase in satellites, while for $M_* > 10^5 M_\odot$ the increase is just 13%.

For an individual halo, the approximate uncertainty from each input for $M_* > 10^4 M_\odot$ is as follows: reionization – 33%, total halo mass – 20%, stellar mass of host – 11%, and SHMF – 11%. We consider the scatter in $M_* - M_{\text{halo}}$ as part of the spectrum of AM models. When combined in quadrature, the uncertainty reaches 42%, commensurate with the differences between abundance matching models, but less

Table 3. Mean number of satellites with $M_* > 10^4 M_\odot$ within a 0.56° radius field of view around Local Group dwarf field galaxies

Name	D_\odot [kpc]	Moster			GK14			GK16			Brook		
		\bar{N}_{lum}	\bar{N}_{fov}	R_{vir} [kpc]	\bar{N}_{lum}	\bar{N}_{fov}	R_{vir} [kpc]	\bar{N}_{lum}	\bar{N}_{fov}	R_{vir} [kpc]	\bar{N}_{lum}	\bar{N}_{fov}	R_{vir} [kpc]
Leo T	417	0.08	0.01	34	0.04	0.01	31	0.03	0.00	30	0.04	0.00	41
And XXVIII	661	0.10	0.02	36	0.06	0.02	33	0.05	0.01	32	0.06	0.01	43
KKR 3	2188	0.16	0.13	41	0.13	0.10	39	0.09	0.07	37	0.10	0.07	48
Tucana	887	0.18	0.05	42	0.13	0.04	40	0.09	0.03	37	0.10	0.02	48
Leo P	1620	0.17	0.10	42	0.13	0.08	40	0.09	0.06	37	0.10	0.05	48
And XVIII	1355	0.18	0.09	42	0.14	0.08	40	0.10	0.05	38	0.11	0.05	49
Phoenix	415	0.20	0.02	43	0.16	0.01	42	0.11	0.01	39	0.11	0.01	50
KKH 86	2582	0.20	0.16	44	0.17	0.14	42	0.12	0.11	39	0.12	0.09	50
Antlia	1349	0.25	0.11	47	0.23	0.10	46	0.15	0.07	43	0.15	0.06	53
KKR 25	1905	0.26	0.16	47	0.24	0.15	46	0.17	0.11	43	0.15	0.08	53
Aquarius	1072	0.28	0.09	48	0.26	0.08	47	0.18	0.06	44	0.16	0.05	54
DDO 113	2951	0.32	0.26	50	0.31	0.26	50	0.21	0.18	46	0.18	0.14	56
Cetus	755	0.36	0.06	52	0.35	0.06	52	0.24	0.05	48	0.20	0.03	57
ESO 294-G010	2032	0.36	0.22	52	0.35	0.21	52	0.24	0.16	48	0.21	0.12	57
Sagittarius dIrr	1067	0.39	0.11	54	0.42	0.11	54	0.29	0.09	51	0.23	0.05	59
ESO 410-G005	1923	0.41	0.23	54	0.41	0.23	54	0.29	0.17	51	0.23	0.12	59
KKH 98	2523	0.46	0.32	56	0.46	0.31	57	0.34	0.25	53	0.25	0.16	60
Leo A	798	0.52	0.08	58	0.55	0.08	60	0.41	0.07	56	0.28	0.04	62
GR 8	2178	0.55	0.32	59	0.58	0.32	61	0.42	0.25	56	0.29	0.16	63
Pegasus dIrr	920	0.55	0.10	59	0.58	0.11	61	0.44	0.09	57	0.29	0.05	63
UGC 9128	2291	0.59	0.34	60	0.65	0.37	63	0.47	0.29	58	0.32	0.18	64
UGC 4879	1361	0.60	0.19	61	0.67	0.21	63	0.50	0.17	59	0.32	0.10	65
KK 258	2230	0.77	0.41	66	0.89	0.45	69	0.68	0.37	65	0.39	0.20	68
UGCA 86	2965	0.81	0.55	67	0.97	0.63	71	0.74	0.50	67	0.41	0.27	69

Table 3 – *continued* Mean number of satellites with $M_* > 10^4 M_\odot$ within a 0.56° radius field of view around Local Group dwarf field galaxies

Name	D_\odot [kpc]	Moster			GK14			GK16			Brook		
		\bar{N}_{lum}	\bar{N}_{fov}	R_{vir} [kpc]	\bar{N}_{lum}	\bar{N}_{fov}	R_{vir} [kpc]	\bar{N}_{lum}	\bar{N}_{fov}	R_{vir} [kpc]	\bar{N}_{lum}	\bar{N}_{fov}	R_{vir} [kpc]
DDO 99	2594	0.82	0.49	67	0.98	0.56	71	0.75	0.45	67	0.40	0.23	69
UKS 2323-326	2208	0.84	0.43	67	0.99	0.48	72	0.77	0.39	68	0.41	0.20	70
UGC 8508	2582	0.90	0.53	69	1.06	0.58	73	0.82	0.48	69	0.44	0.25	71
KKs 3	2120	0.97	0.45	70	1.22	0.52	76	0.92	0.42	72	0.46	0.21	72
NGC 4163	2858	1.17	0.69	75	1.56	0.84	82	1.22	0.70	78	0.56	0.33	76
WLM	933	1.26	0.16	77	1.69	0.18	85	1.32	0.16	80	0.58	0.07	77
Sextans A	1432	1.28	0.32	77	1.70	0.37	85	1.33	0.31	81	0.60	0.15	78
DDO 125	2582	1.31	0.68	78	1.73	0.81	86	1.41	0.70	82	0.61	0.31	78
DDO 190	2793	1.37	0.76	79	1.87	0.94	87	1.47	0.77	83	0.63	0.35	79
Sextans B	1426	1.40	0.33	79	1.86	0.38	87	1.48	0.33	83	0.64	0.15	79
IC 3104	2270	1.49	0.64	81	2.03	0.77	90	1.63	0.65	86	0.67	0.29	81
NGC 3109	1300	1.65	0.31	84	2.29	0.37	93	1.85	0.32	89	0.75	0.14	83
NGC 6822	459	1.85	0.05	87	2.61	0.07	98	2.09	0.05	94	0.82	0.02	86
IC 1613	755	1.84	0.14	87	2.60	0.16	98	2.16	0.14	94	0.81	0.06	86
IC 4662	2443	2.46	0.95	95	3.61	1.18	109	2.96	1.02	105	1.10	0.43	94
IC 5152	1950	2.81	0.75	100	4.28	0.94	115	3.74	0.84	113	1.29	0.35	99

Note. — \bar{N}_{fov} indicates the mean number of luminous satellites with $M_* > 10^4 M_\odot$ within a field of view of radius 0.56° (corresponding to a footprint of equal area as the Solo Dwarfs Project) centered on target Local Group dwarf galaxies, as predicted with various AM models. Galaxies with a larger heliocentric distance and smaller AM model inferred virial radius, R_{vir} , will have a larger fraction of their volume surveyed in the field of view. The total mean number of satellites within each galaxy’s virial volume, \bar{N}_{lum} , is listed for comparison.

than the Poisson noise of systems with $\bar{N}_{\text{lum}} \leq 4$. Since uncertainty in total halo mass and stellar mass are not fully correlated from one halo to the next, their contribution can be mitigated by observing a larger sample of galaxies.

Consequently, the dominant contributors to uncertainty are the abundance matching model, reionization, and Poisson noise. While Poisson noise is uncontrollable, reionization and AM models will improve with future observations and better models. For satellites with $10^3 < M_* < 10^4 M_\odot$, uncertainty in reionization is the single most important model dependent factor. However, for satellites with $M_* > 10^5 M_\odot$, reionization has little influence, and differences between abundance matching models dominate.

Although uncertainties are large, even the most conservative estimates for the existence of satellites suggest that at least one satellite with $M_* > 10^4$ exists around the largest field dwarf galaxies. For $M_* > 10^5 M_\odot$, the lowest estimate comes from the Brook model with a combined uncertainty from reionization, halo mass, stellar mass, and SHMF of 15% for the number of satellites around the five largest field dwarfs. Here, reionization only makes a 2% contribution on its own. Reducing the mean expected predictions by 15% and including Poisson noise, this lower limit still predicts an 88% chance that at least one satellite with $M_* > 10^5 M_\odot$ exists around one of the targets.

6 CONCLUSIONS

We have made predictions for the number of luminous satellites around galaxies using SHMFs derived from the *Caterpillar* simulation suite, a model for reionization, and four different AM methods. We find the number of satellites as a function of their minimum stellar mass as well as their host galaxy's total stellar mass. We predict a combined ~ 70 ultrafaint and classical satellites ($M_*^{\text{sat}} > 10^3 M_\odot$) around a MW-sized galaxy, consistent with observational expectations. This result is devoid of any missing satellite problem.

For the more massive isolated Local Group dwarf field galaxies, our predictions overwhelmingly indicate that at least one satellite with $M_* > 10^5 M_\odot$ exists, and that many exist with $M_* > 10^4 M_\odot$. Specifically, when observing the virial volumes of the five largest field galaxies combined, there is a $> 99\%$ chance of discovering at least one satellite with $M_* > 10^5 M_\odot$, when employing the AM models of Moster, GK14, and GK16, each paired with a reionization model. The existence of at least one such satellite is even supported by our most conservative case, i.e. using the Brook model that underpredicts the number of MW satellites by $\approx 2\sigma$ compared to other AM models. The Brook model still predicts a $92 \pm 4\%$ chance of one satellite with $M_* > 10^5 M_\odot$ within the combined virial volumes of the five largest field galaxies, IC 5152, IC 4662, IC 1613, NGC 6822 and NGC 3109. If probing down to $M_*^{\text{sat}} > 10^4 M_\odot$, 5 – 25 satellites may even exist.

We therefore conclude that deep, wide-field searches for faint ($10^3 < M_* < 10^6 M_\odot$) satellites around the known, isolated Local Group field dwarf galaxies should result in the discovery of satellites. This bears the opportunity to study satellites that would likely have environments different from any of the known MW or M31 satellites. A smaller mass host implies they would experience reduced ram pressure strip-

Table 4. Systematic Errors

Parameter Change	% change in \bar{N}_{lum}^5	
	$M_* > 10^4 M_\odot$	$M_* > 10^3 M_\odot$
Reionization at $z = 14.4$	−5	−12
Reionization at $z = 11.3$	8	26
Reionization at $z = 9.3$	20	65
$v_{\text{max}}^{\text{filt}}, v_{\text{max}}^{\text{pre}} \uparrow 25\%$	−38	−47
$v_{\text{max}}^{\text{filt}}, v_{\text{max}}^{\text{pre}} \downarrow 25\%$	27	70
$M_{\text{halo}}^{\text{host}} \uparrow 22\%$	23	26
$M_{\text{halo}}^{\text{host}} \downarrow 18\%$	−18	26
$M_*^{\text{host}} \uparrow 25\%$	10	10
$M_*^{\text{host}} \downarrow 25\%$	−12	−12
$M_{200}^{\text{infall}} \text{ SHMF } \alpha = 1.88$	−12	−9
$M_{200}^{\text{infall}} \text{ SHMF } \alpha = 1.75$	10	8
GK16, $\gamma = 0.0$	24	5
GK16, $\gamma = -0.5$	−32	−24
$t_{\text{infall}} \uparrow 0.23 \text{ Gyr}$	< 1	< 1
$t_{\text{infall}} \downarrow 0.23 \text{ Gyr}$	< 1	< 1

Note. — Systematic uncertainties in model input variables and their effect on the predicted number of luminous satellites. Percent change is reported on \bar{N}_{lum}^5 , the mean number of satellites with $M_* > 10^4 M_\odot$ found around the largest five galaxies for the Moster model. The values in the final column refer to satellites with $M_* > 10^3 M_\odot$. Adjusting scatter, γ , in the $M_* - M_{\text{halo}}$ relationship applies only to the GK16 model. More negative values of γ indicate more scatter. Our baseline reionization occurs at $z = 13.3$, our baseline α in the SHMF is 1.81, and our baseline γ is -0.2 . $v_{\text{max}}^{\text{filt}}$ is the maximum circular velocity of halos above which all halos are assumed to have formed stars, regardless of when this v_{max} was reached. $v_{\text{max}}^{\text{pre}}$ is the maximum circular velocity of halos which, if reached by the redshift of reionization, indicates star formation will proceed.

ping, reduced tidal forces, and a different local reionization field. An additional implication is that the MW satellites Fornax ($M_* = 2.5 \times 10^7 M_\odot$) and Sagittarius ($M_* \sim 10^8 M_\odot$ at infall; [Niederste-Ostholt et al. 2010](#)) more likely than not had one own small satellite galaxy before getting accreted by the MW. Along the same vein, predictions for the numbers of satellites expected around the SMC and LMC will be reported on in a separate paper.

We estimate how many satellites are in an observable line of sight of specific Local Group galaxies as a function of the radius of the field of view. Making specific predictions will help ensure that the most promising targets are observed to avoid spending significant amounts of telescope time on many (potentially unnecessary) pointings to cover the full virial volume of a given field galaxy. We explicitly calculate expected numbers for galaxies included in the Solo dwarf survey [Higgs et al. \(2016\)](#), which has recently observed all

isolated dwarf field galaxies within 3 Mpc of the MW. For instance, a single pointing at IC 4662 with their $1^\circ \times 1^\circ$ camera would cover a volume that encompasses a mean of $\sim 0.9 - 1.2$ satellites with $M_* > 10^4 M_\odot$ according to the Moster, GK16, and GK14 models. No satellites of dwarfs have been reported yet in the Solo survey, but given our predictions, we expect that some will be found in their fields of view.

In order to maximize chances of discovering as many satellites as possible, we find the best observing strategy to be to search within small radii of the largest galaxies. After all, the density of satellites is much higher towards their galactic centers than the outskirts. In addition, multiple galaxies should be surveyed this way since observing just one galaxy could yield a non-detection of satellites if it were to have an unusually low halo mass for its stellar mass. If results from a complete survey of all field dwarfs would be available, especially if observations would also cover the full virial volumes of many galaxies including the MW and M31, constraints on the epoch of reionization and the various AM models could be derived.

AM models contribute a large $\sim 50\%$ uncertainty relative to the Moster model to the predictions of satellite abundances. Reionization, which preferentially suppresses star formation in low mass galaxies, can contribute up to 70% uncertainty for $M_*^{\text{sat}} > 10^3 M_\odot$, but only $\sim 10\%$ for $M_*^{\text{sat}} > 10^5 M_\odot$. Measurements to a completeness limit of $10^5 M_\odot$ would primarily constrain the $M_* - M_{\text{halo}}$ relationship for galaxies and thus the accuracy of the abundance matching models. If observations could ever yield a census of satellites down to $10^3 M_\odot$, reionization could also be constrained by placing limits on the ability of reionization to suppress (or not) star formation in these small halos.

Finally, we emphasize that discovering no satellites at all is highly unlikely. Nevertheless, a non-detection would imply at least two of the following: a very strong suppression of star formation by reionization, a low $M_* - M_{\text{halo}}$ relationship for low mass galaxies, a high $M_* - M_{\text{halo}}$ relationship for galaxies with masses typical of field dwarfs, and a MW which has an abnormally large number of luminous satellites with $M_* < 10^6 M_\odot$. We therefore conclude that there are almost certainly many small satellites of dwarf galaxies waiting to be discovered and that their discovery will help refine not just AM models and reionization but our understanding of low mass galaxy formation.

ACKNOWLEDGEMENTS

G.A.D. acknowledges support from an NSF Graduate Research Fellowship under Grant No. 1122374. Support for A.H.G.P. was provided in part by NASA through the HST theory grant HST-AR-13896.005-A from the Space Telescope Science Institute, which is operated by the Association of Universities for Research in Astronomy, Inc., under NASA contract NAS 5-26555. BW acknowledges support by NSF Faculty Early Career Development (CAREER) award AST-1151462. We thank Shea Garrison-Kimmel for private correspondence regarding abundance matching implementations, and Chris Barber for providing data we used for our default reionization model.

REFERENCES

- Barber C., Starkenburg E., Navarro J. F., McConnachie A. W., Fattahi A., 2014, *MNRAS*, **437**, 959
- Barkana R., Loeb A., 1999, *ApJ*, **523**, 54
- Bechtol K., et al., 2015, *ApJ*, **807**, 50
- Behroozi P. S., Wechsler R. H., Wu H.-Y., Busha M. T., Klypin A. A., Primack J. R., 2013a, *ApJ*, **763**, 18
- Behroozi P. S., Wechsler R. H., Conroy C., 2013b, *ApJ*, **770**, 57
- Bell E. F., Slater C. T., Martin N. F., 2011, *ApJ*, **742**, L15
- Belokurov V., et al., 2006, *ApJ*, **647**, L111
- Belokurov V., et al., 2007, *ApJ*, **654**, 897
- Belokurov V., et al., 2008, *ApJ*, **686**, L83
- Belokurov V., et al., 2009, *MNRAS*, **397**, 1748
- Belokurov V., et al., 2010, *ApJ*, **712**, L103
- Benson A. J., Frenk C. S., Lacey C. G., Baugh C. M., Cole S., 2002, *MNRAS*, **333**, 177
- Bovill M. S., Ricotti M., 2009, *ApJ*, **693**, 1859
- Bovill M. S., Ricotti M., 2011a, *ApJ*, **741**, 17
- Bovill M. S., Ricotti M., 2011b, *ApJ*, **741**, 18
- Boylan-Kolchin M., Springel V., White S. D. M., Jenkins A., Lemson G., 2009, *MNRAS*, **398**, 1150
- Boylan-Kolchin M., Springel V., White S. D. M., Jenkins A., 2010, *MNRAS*, **406**, 896
- Bromm V., Yoshida N., 2011, *ARA&A*, **49**, 373
- Brook C. B., Di Cintio A., Knebe A., Gottlöber S., Hoffman Y., Yepes G., Garrison-Kimmel S., 2014, *ApJ*, **784**, L14
- Brown T. M., et al., 2012, *ApJ*, **753**, L21
- Brown T. M., et al., 2014a, *Mem. Soc. Astron. Italiana*, **85**, 493
- Brown T. M., et al., 2014b, *ApJ*, **796**, 91
- Bryan G. L., Norman M. L., 1998, *ApJ*, **495**, 80
- Bullock J. S., Kravtsov A. V., Weinberg D. H., 2000, *ApJ*, **539**, 517
- Busha M. T., Wechsler R. H., Behroozi P. S., Gerke B. F., Klypin A. A., Primack J. R., 2011, *ApJ*, **743**, 117
- Carlin J. L., et al., 2016, preprint, ([arXiv:1608.02591](https://arxiv.org/abs/1608.02591))
- Crnojević D., et al., 2016, *ApJ*, **823**, 19
- Dooley G. A., Griffen B. F., Zukin P., Ji A. P., Vogelsberger M., Hernquist L. E., Frebel A., 2014, *ApJ*, **786**, 50
- Dooley G. A., Peter A. H. G., Vogelsberger M., Zavala J., Frebel A., 2016, *MNRAS*, **461**, 710
- Drlica-Wagner A., et al., 2015, *ApJ*, **813**, 109
- Drlica-Wagner A., et al., 2016, preprint, ([arXiv:1609.02148](https://arxiv.org/abs/1609.02148))
- Efstathiou G., 1992, *MNRAS*, **256**, 43P
- Eisenstein D. J., Hu W., 1998, *ApJ*, **496**, 605
- Elbert O. D., Bullock J. S., Garrison-Kimmel S., Rocha M., Oñorbe J., Peter A. H. G., 2015, *MNRAS*, **453**, 29
- Frebel A., Bromm V., 2012, *ApJ*, **759**, 115
- Frenk C. S., White S. D. M., 2012, *Annalen der Physik*, **524**, 507
- Gao L., De Lucia G., White S. D. M., Jenkins A., 2004a, *MNRAS*, **352**, L1
- Gao L., White S. D. M., Jenkins A., Stoehr F., Springel V., 2004b, *MNRAS*, **355**, 819
- Garrison-Kimmel S., Boylan-Kolchin M., Bullock J. S., Lee K., 2014, *MNRAS*, **438**, 2578
- Garrison-Kimmel S., Bullock J. S., Boylan-Kolchin M., Bardwell E., 2016, preprint, ([arXiv:1603.04855](https://arxiv.org/abs/1603.04855))
- Gnedin N. Y., 2000, *ApJ*, **542**, 535
- Gottloeber S., Hoffman Y., Yepes G., 2010, preprint, ([arXiv:1005.2687](https://arxiv.org/abs/1005.2687))
- Griffen B. F., Dooley G. A., Ji A. P., O’Shea B. W., Gómez F. A., Frebel A., 2016a, preprint, ([arXiv:1611.00759](https://arxiv.org/abs/1611.00759))
- Griffen B. F., Ji A. P., Dooley G. A., Gómez F. A., Vogelsberger M., O’Shea B. W., Frebel A., 2016b, *ApJ*, **818**, 10
- Guo Q., White S., Li C., Boylan-Kolchin M., 2010, *MNRAS*, **404**, 1111
- Han J., Cole S., Frenk C. S., Jing Y., 2016, *MNRAS*, **457**, 1208
- Hargis J. R., Willman B., Peter A. H. G., 2014, *ApJ*, **795**, L13

- Higgs C. R., et al., 2016, *MNRAS*, **458**, 1678
- Irwin M. J., et al., 2007, *ApJ*, **656**, L13
- Irwin M. J., Ferguson A. M. N., Huxor A. P., Tanvir N. R., Ibata R. A., Lewis G. F., 2008, *ApJ*, **676**, L17
- Jang I. S., Lee M. G., 2014, *ApJ*, **795**, L6
- Ji A. P., Frebel A., Chiti A., Simon J. D., 2016, *Nature*, **531**, 610
- Karachentsev I. D., Makarova L. N., Tully R. B., Wu P.-F., Kniazev A. Y., 2014, *MNRAS*, **443**, 1281
- Karachentsev I. D., Makarova L. N., Makarov D. I., Tully R. B., Rizzi L., 2015, *MNRAS*, **447**, L85
- Kim D., Jerjen H., 2015, *ApJ*, **808**, L39
- Kim D., Jerjen H., Mackey D., Da Costa G. S., Milone A. P., 2015, *ApJ*, **804**, L44
- Kirby E. N., Simon J. D., Geha M., Guhathakurta P., Frebel A., 2008, *ApJ*, **685**, L43
- Klypin A., Kravtsov A. V., Valenzuela O., Prada F., 1999, *ApJ*, **522**, 82
- Klypin A. A., Trujillo-Gomez S., Primack J., 2011, *ApJ*, **740**, 102
- Koposov S. E., Belokurov V., Torrealba G., Evans N. W., 2015, *ApJ*, **805**, 130
- Kravtsov A., 2010, *Advances in Astronomy*, **2010**, 281913
- Kravtsov A. V., Berlind A. A., Wechsler R. H., Klypin A. A., Gottlöber S., Allgood B., Primack J. R., 2004, *ApJ*, **609**, 35
- Laevens B. P. M., et al., 2015, *ApJ*, **813**, 44
- Lu Y., Benson A., Mao Y.-Y., Tonnesen S., Peter A. H. G., Wetzel A. R., Boylan-Kolchin M., Wechsler R. H., 2016, preprint, ([arXiv:1605.02075](https://arxiv.org/abs/1605.02075))
- Lunnan R., Vogelsberger M., Frebel A., Hernquist L., Lidz A., Boylan-Kolchin M., 2012, *ApJ*, **746**, 109
- Luque E., et al., 2016, preprint, ([arXiv:1608.04033](https://arxiv.org/abs/1608.04033))
- Madau P., Kuhlen M., Diemand J., Moore B., Zemp M., Potter D., Stadel J., 2008, *ApJ*, **689**, L41
- Majewski S. R., et al., 2007, *ApJ*, **670**, L9
- Mao Y.-Y., Williamson M., Wechsler R. H., 2015, *ApJ*, **810**, 21
- Martin N. F., et al., 2009, *ApJ*, **705**, 758
- Martin N. F., et al., 2015, *ApJ*, **804**, L5
- McConnachie A. W., 2012, *AJ*, **144**, 4
- McConnachie A. W., et al., 2008, *ApJ*, **688**, 1009
- McConnachie A. W., et al., 2009, *Nature*, **461**, 66
- McQuinn K. B. W., et al., 2015, *ApJ*, **812**, 158
- Moore B., Ghigna S., Governato F., Lake G., Quinn T., Stadel J., Tozzi P., 1999, *ApJ*, **524**, L19
- More S., Diemer B., Kravtsov A. V., 2015, *ApJ*, **810**, 36
- Moster B. P., Somerville R. S., Maulbetsch C., van den Bosch F. C., Macciò A. V., Naab T., Oser L., 2010, *ApJ*, **710**, 903
- Moster B. P., Naab T., White S. D. M., 2013, *MNRAS*, **428**, 3121
- Munshi F., et al., 2013, *ApJ*, **766**, 56
- Niederste-Ostholt M., Belokurov V., Evans N. W., Peñarrubia J., 2010, *ApJ*, **712**, 516
- Norris J. E., Gilmore G., Wyse R. F. G., Yong D., Frebel A., 2010, *ApJ*, **722**, L104
- Oñorbe J., Hennawi J. F., Lukić Z., 2016, preprint, ([arXiv:1607.04218](https://arxiv.org/abs/1607.04218))
- O'Shea B. W., Wise J. H., Xu H., Norman M. L., 2015, *ApJ*, **807**, L12
- Okamoto T., Frenk C. S., 2009, *MNRAS*, **399**, L174
- Okamoto T., Gao L., Theuns T., 2008, *MNRAS*, **390**, 920
- Pawlik A. H., Schaye J., 2009, *MNRAS*, **396**, L46
- Peter A. H. G., Benson A. J., 2010, *Phys. Rev. D*, **82**, 123521
- Pillepich A., et al., 2014, *MNRAS*, **444**, 237
- Power C., Wynn G. A., Robotham A. S. G., Lewis G. F., Wilkinson M. I., 2014, preprint, ([arXiv:1406.7097](https://arxiv.org/abs/1406.7097))
- Richardson J. C., et al., 2011, *ApJ*, **732**, 76
- Riebe K., et al., 2011, preprint, ([arXiv:1109.0003](https://arxiv.org/abs/1109.0003))
- Roediger J. C., Courteau S., 2015, *MNRAS*, **452**, 3209
- Sales L. V., Wang W., White S. D. M., Navarro J. F., 2013, *MNRAS*, **428**, 573
- Sand D. J., et al., 2014, *ApJ*, **793**, L7
- Sand D. J., Spekkens K., Crnojević D., Hargis J. R., Willman B., Strader J., Grillmair C. J., 2015, *ApJ*, **812**, L13
- Sawala T., Frenk C. S., Crain R. A., Jenkins A., Schaye J., Theuns T., Zavala J., 2013, *MNRAS*, **431**, 1366
- Sawala T., et al., 2015, *MNRAS*, **448**, 2941
- Sawala T., et al., 2016, *MNRAS*, **456**, 85
- Shapiro P. R., Iliev I. T., Raga A. C., 2004, *MNRAS*, **348**, 753
- Shapley H., 1922, Harvard College Observatory Bulletin, **775**, 1
- Shapley H., 1924, Harvard College Observatory Circular, **268**, 1
- Sheth R. K., Tormen G., 2002, *MNRAS*, **329**, 61
- Slater C. T., Bell E. F., Martin N. F., 2011, *ApJ*, **742**, L14
- Somerville R. S., 2002, *ApJ*, **572**, L23
- Springel V., et al., 2005, *Nature*, **435**, 629
- Springel V., et al., 2008, *MNRAS*, **391**, 1685
- Starkenburg E., et al., 2013, *MNRAS*, **429**, 725
- Tasitsiomi A., Kravtsov A. V., Wechsler R. H., Primack J. R., 2004, *ApJ*, **614**, 533
- Tegmark M., Silk J., Rees M. J., Blanchard A., Abel T., Palla F., 1997, *ApJ*, **474**, 1
- Thoul A. A., Weinberg D. H., 1996, *ApJ*, **465**, 608
- Torrealba G., et al., 2016, preprint, ([arXiv:1605.05338](https://arxiv.org/abs/1605.05338))
- Ural U., Wilkinson M. I., Read J. I., Walker M. G., 2015, *Nature Communications*, **6**, 7599
- Vale A., Ostriker J. P., 2004, *MNRAS*, **353**, 189
- Vale A., Ostriker J. P., 2006, *MNRAS*, **371**, 1173
- Walsh S. M., Jerjen H., Willman B., 2007, *ApJ*, **662**, L83
- Walsh S. M., Willman B., Jerjen H., 2009, *AJ*, **137**, 450
- Wang L., Jing Y. P., 2010, *MNRAS*, **402**, 1796
- Wang W., Han J., Cooper A. P., Cole S., Frenk C., Lowing B., 2015, *MNRAS*, **453**, 377
- Wheeler C., Oñorbe J., Bullock J. S., Boylan-Kolchin M., Elbert O. D., Garrison-Kimmel S., Hopkins P. F., Kereš D., 2015, *MNRAS*, **453**, 1305
- Wiersma R. P. C., Schaye J., Smith B. D., 2009, *MNRAS*, **393**, 99
- Willman B., et al., 2005a, *AJ*, **129**, 2692
- Willman B., et al., 2005b, *ApJ*, **626**, L85
- Yang X., Mo H. J., van den Bosch F. C., 2003, *MNRAS*, **339**, 1057
- Yang X., Mo H. J., van den Bosch F. C., Zhang Y., Han J., 2012, *ApJ*, **752**, 41
- Zijlstra A. A., Minniti D., 1999, *AJ*, **117**, 1743
- Zucker D. B., et al., 2004, *ApJ*, **612**, L121
- Zucker D. B., et al., 2006a, *ApJ*, **643**, L103
- Zucker D. B., et al., 2006b, *ApJ*, **650**, L41
- Zucker D. B., et al., 2007, *ApJ*, **659**, L21
- de Blok W. J. G., 2010, *Advances in Astronomy*, **2010**, 789293
- van den Bosch F. C., Tormen G., Giocoli C., 2005, *MNRAS*, **359**, 1029